Fire Performance Evaluation of Building Integrated Photovoltaic (BIPV) Façade Systems

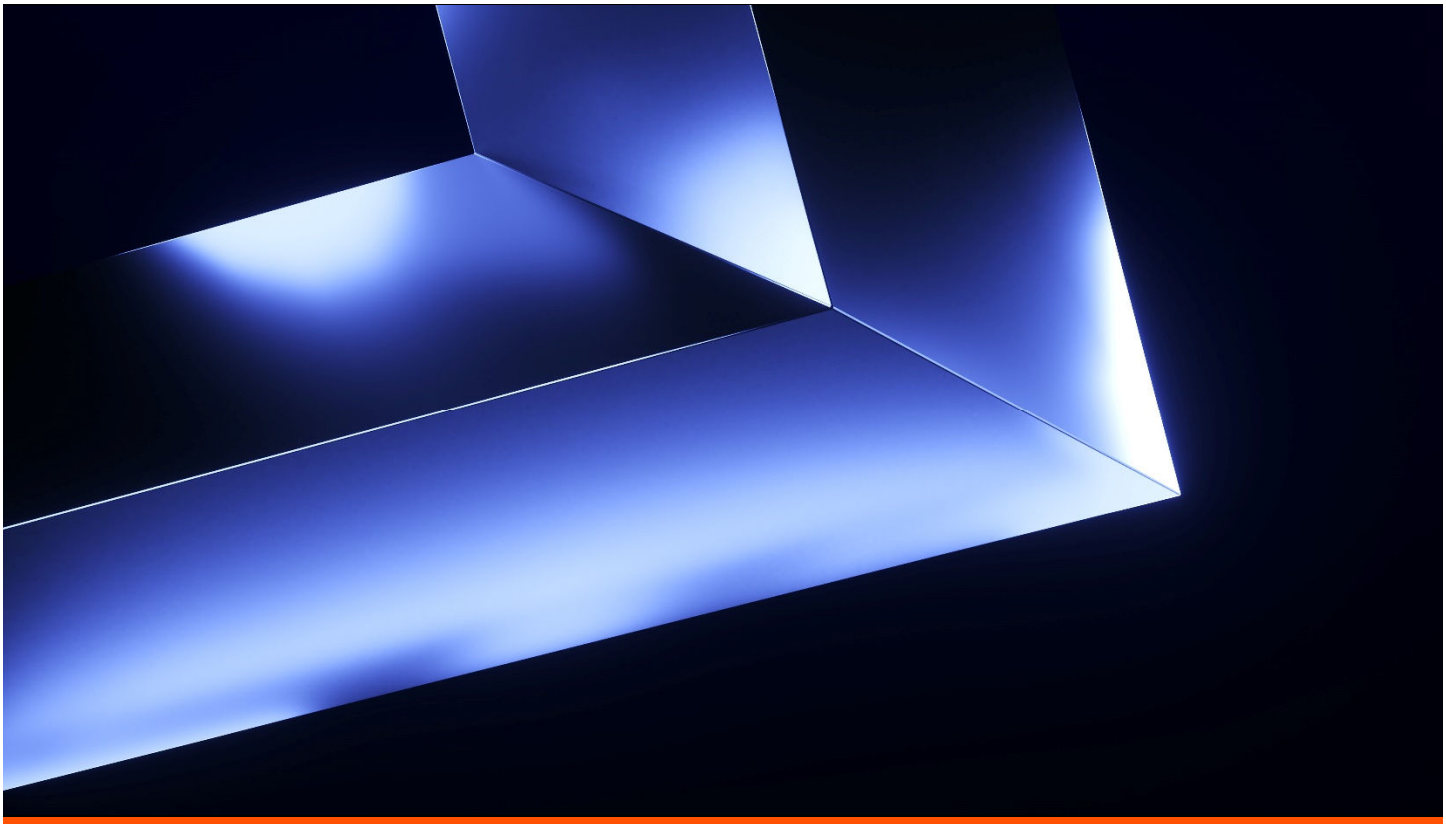

TECHNICAL REPORT

Fire Performance Evaluation of Building Integrated Photovoltaic (BIPV) Façade Systems

Prepared by

Gaurav Agarwal

FM
One Technology Way, Norwood, MA 02062

November 2025

Project ID: RW000606

Disclaimer

The research presented in this report, including any findings and conclusions, is for informational purposes only. Any references to specific products, manufacturers, or contractors do not constitute a recommendation, evaluation or endorsement by Factory Mutual Insurance Company (FM) of such products, manufacturers or contractors. FM does not address life, safety, or health issues. The recipient of this report must make the decision whether to take any action. FM undertakes no duty to any party by providing this report or performing the activities on which it is based. FM makes no warranty, express or implied, with respect to any product or process referenced in this report. FM assumes no liability by or through the use of any information in this report.

Executive Summary

Building-integrated photovoltaic (BIPV) façade systems are a type of cavity wall construction that utilizes PV modules as cladding. These systems serve the dual purpose of functioning as high-performance building envelopes and generating electricity. Despite their advantages, BIPV façade systems and their components, such as PV modules, electrical cables, and junction boxes, are combustible. Furthermore, when mounted outdoors as façades, the electrically charged state of PV modules can increase the flammability of the wall system. This study investigates the fire hazards associated with various BIPV façade systems using large-scale façade fire tests outlined in the ANSI/FM 4411[i] standard. It also examines the impact of the charged state of BIPV modules on fire test results. These findings contribute to the development of large-scale testing guidelines to evaluate the fire performance of BIPV façade systems.

BIPV cladding modules typically consist of encapsulated solar cells between two layers of high-strength tempered glass, each approximately 2 to 6 mm thick, serving as the superstrate and substrate. Thin films of combustible plastic sheets, such as ethylene vinyl acetate (EVA) or polyolefin (POE), about 0.2 to 1 mm thick, encapsulate and insulate the solar cell from the glass layers. The air cavity between the BIPV modules and the insulation backing is usually 2 to 6 in. (50 to 150 mm) deep, allowing air ventilation and rainwater drainage. This cavity also contains several electrical components, including cables, junction boxes, and inverters, which can be combustible.

In this study, four BIPV cavity wall façades were selected, each differing in aspects such as glass thickness, module size, solar cell technology, encapsulant type, and power rating. BIPV façade systems, representative of field installations, were constructed for large-scale fire testing. Two-inch (50 mm) thick non-combustible insulation was used behind the air cavity, which was 4 to 4.75 in. (100 to 120 mm) deep, with interconnected electrical cables to simulate realistic installations. In addition, a single self-adhering flexible BIPV module was tested by mounting it directly onto non-combustible gypsum sheathing.

The BIPV systems were tested using two large-scale fire test methods specified in the ANSI/FM 4411 standard for cavity wall constructions. The primary method is the ISO 3957[ii] standard, commonly known as the 16 ft (4.9 m) high parallel panel test (16-ft PPT), which simulates fire scenarios such as exterior and post-flashover fires. The second method is the 8 ft (2.4 m) high cavity wall test (8-ft CWT), designed to simulate fire scenarios originating within a wall cavity, such as electrical fires, welding fires, and flying embers, among others. The tests were conducted with BIPV modules in both uncharged and maximum-rated power (MP) charged states.

The 16-ft PPT results for uncharged BIPV cavity wall façade systems effectively captured the relevant fire spread dynamics. A few minutes after the test began, the high heat flux from propane flames caused the bottommost BIPV glass modules to shatter. This allowed flames to enter the cavity and accelerate fire propagation as combustible gases from cables and plastic encapsulants were released following the breakage of glass substrates. As the fire spread upward within the cavity, flames escaped through various joint openings to the exterior, ultimately leading to the burning of adhesives used to mount the modules and resulting in significant glass debris falling onto the weighing platform. The falling and shattering of BIPV modules onto the propane burner ignited the combustible plastic encapsulants. The results underscored the importance of evaluating the complete BIPV façade system—including PV modules, interconnected cables, insulation, air cavity, and mounting system—to accurately assess flame spread hazards.

The 16-ft PPT results of BIPV façade systems at MP charge conditions showed varied outcomes. Tests with modules consisting of 4 mm thick superstrate glass revealed higher fire hazards compared to the uncharged counterparts. These tests revealed faster fire propagation within the cavity and peak heat release rates (HRR) that were 50 to 60% higher than those measured in uncharged façade tests. The increased fire hazard was attributed to the greater tendency of the BIPV glass to shatter due to charging-induced preheating. However, test results for BIPV systems with thicker, 6 mm glass superstrates did not exhibit such differences between charged and uncharged conditions. This is likely due to the minimal preheating effects, attributed to their higher heat capacity.

[i] ANSI/FM 4411-2020, *American National Standard for Cavity Wall Systems*. Norwood, MA, USA: FM Approvals LLC, 2020.

[ii] ISO 3957, *Reaction to Fire Tests — Parallel Panel Test Method for Wall Systems — Measurement of Heat Release and Smoke Production*. Geneva, Switzerland: International Organization for Standardization, 2025.

The results from the flexible BIPV tests revealed accelerated flame spread, with a maximum flame height greater than 30 ft (9.1 m). The peak HRR reached approximately 11 MW within 100 s of ignition for both uncharged and MP charged tests. Unlike the double-sided glass BIPV cavity-wall systems, the flexible BIPV's laminated plastic superstrate caused the surface flame spread to dominate the vertical fire growth.

The final assessment of the fire performance of BIPV façades remains consistent regardless of their charging status. Façades that perform well or exhibit fire propagation in an uncharged state maintain these outcomes even when charged. Consequently, it is recommended to test the BIPV systems under uncharged conditions.

None of the double-sided glass BIPV systems evaluated in this study showed fire spread in the 8-ft CWT configuration. The propane burner exposure was insufficient to shatter the tempered glass and release its plastic encapsulants, which eventually drove the fire dynamics observed in the 16-ft PPTs. It is therefore recommended to exempt double-sided glass BIPVs from 8-ft CWTs.

The comprehensive recommendations for developing an FM Approval standard, FM 4483 for wall-mounted BIPV systems, are detailed in Section 8. The major highlights of these recommendations are summarized as follows:

1. **BIPV cavity wall systems**
   a. Recommended test: 16-ft PPT of the entire façade system (including connected cables) in its uncharged state.
      Pass criteria: Systems must meet all of the following three criteria
      I. Peak HRR ≤ 830 kW for unlimited height and 830 kW < peak HRR ≤ 1100 kW for 50-ft (15 m) height installation.
      II. Peak cavity temperature at 12 ft (3.7 m) height ≤ 473 K (200 °C).
      III. Top 4 ft (1.2 m) of PV modules remain undamaged, i.e. no cracking or shattering.

   b. Recommended test: (in addition to a. above, if the cavity insulation, the BIPV substrate, or both are combustible) 8-ft CWT in uncharged state.
      Pass criteria: follow the performance criteria of 8-ft CWT in ANSI/FM 4411.

2. **Flexible self-adhered BIPV modules**
   a. Recommended test: 16-ft PPT of the entire façade system (including connected cables) in its uncharged state
      Pass criteria: follow the performance criteria of ANSI/FM 4880[iii].

[iii] ANSI/FM 4880-2017, *American National Standard for Evaluating the Fire Performance of Insulated Building Panel Assemblies and Interior Finish Materials*. Norwood, MA, USA: FM Approvals LLC, 2024.

Abstract

The primary objective of this research is to investigate the fire performance of various building-integrated photovoltaic (BIPV) façades using the large-scale fire tests specified in ANSI/FM 4411. Furthermore, this study evaluates the effect of the charged status, which simulates the heating of BIPV modules by sunlight, on the results of the fire tests.

To this end, four BIPV cavity-wall systems, comprising different double-sided glass (bifacial) PV modules, are evaluated for their fire performance using the two test methods of ANSI/FM 4411; namely, the 16-ft high parallel panel test (16-ft PPT) and the 8-ft high cavity wall test (8-ft CWT). The 16-ft PPT effectively captures the flame spread dynamics of BIPV cavity-wall systems. The tests reveal that the primary hazards are related to cavity fire spread, shattering of BIPV glass, burning of plastic encapsulants, and falling debris. The study underscores the importance of assessing the complete BIPV cavity-wall system—including PV modules, and cavity details such as electrical cables, insulation, air cavity depth, and mounting systems—to accurately evaluate flame spread hazards.

Based on the testing results and analysis, recommendations are provided for using the 16-ft PPT and 8-ft CWT for evaluating BIPV façade systems, with changes to the pass/failure criteria and enhanced instrumentation requirements compared to those listed in ANSI/FM 4411.

Acknowledgements

The author gratefully acknowledges the FM Research Campus Staff for carrying out the tests; Timothee Rodrique, Joanna Blaney, Dr. Sujit Purushothaman, Dr. Dong Zeng, Dr. Marcos Chaos, Dr. Yi Wang, and Dr. Sergey Dorofeev for their helpful input and discussions during the course of this work; and all reviewers for their insightful comments and recommendations.

Table of Contents

List of Figures

List of Tables

1. Introduction

Building-integrated photovoltaic (BIPV) systems are emerging as popular and modern PV construction solutions. By definition [1, 2], BIPV systems are integral elements of buildings, serving the dual purpose of fulfilling construction and electrical power generation requirements. The design of a building occurs around the BIPV system, meaning that the construction, functionality, and fire safety of BIPV systems determine the building's overall performance in terms of local codes related to life safety, fire safety, energy efficiency, electrical standards, and more. The most common applications of BIPV systems include façades, skylights, roof shingles, walkable roof tiles, and PV glass curtain walls (see-through walls). In contrast, building-attached photovoltaic (BAPV) systems, such as roof-mounted solar modules, can be added-to or removed-from an existing building without affecting its construction functionality. Figure 1-1 provides examples of common BIPV and BAPV systems.

(a) roof-mounted BAPV system

(b) BIPV façade (photo courtesy of Onyx Solar)

(c) BIPV glass curtainwalls (photos courtesy of Onyx Solar)

(d) BIPV roof shingles (photo courtesy of Onyx Solar)

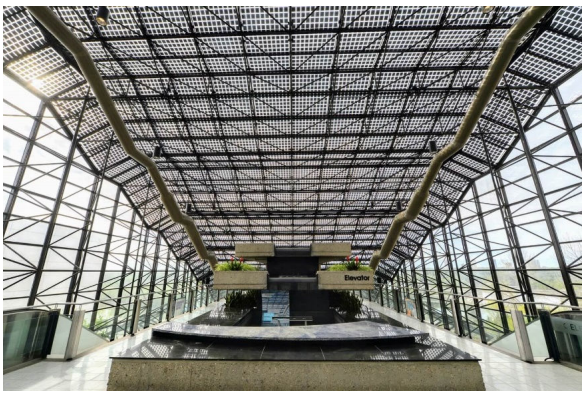

(e) BIPV skylights (photo courtesy of Onyx Solar)

(f) BIPV roof-tiles (photo courtesy of Onyx Solar)

Figure 1-1: Examples of BIPV and BAPV systems.

Among BIPV systems, BIPV cavity-wall façades are considered a part of the high-performance building envelope category. These façades consist of several components, including PV modules, insulation, weather barriers, electrical cables, junction boxes, and mounting systems. Figure 1-2 illustrates examples of BIPV cavity-wall façade systems along with their components. These façades are modular in construction, allowing various component manufacturers to collaborate in developing a wall system tailored to the specific needs of a building. As a result, BIPV façades are increasingly used in high-rise buildings due to their aesthetic appeal, modularity, energy-saving advantages, and power generation benefits.

(a) BIPV module used in cavity wall systems

(b) BIPV cavity-wall façade with components cutout

(c) BIPV cavity wall facade

Figure 1-2: Examples of BIPV cavity-wall facade systems and its components in a cavity wall system.

Despite their benefits, BIPV façade systems and their components can be combustible, which may lead to fire propagation. The past decades have seen numerous high-rise building fires [2], including the tragic events at Grenfell Tower in London [3] and the Valencia fires [4], among others, resulting in significant loss of life and property. Façade fires remain a persistent issue worldwide, leading to scrutiny and modifications of various façade fire testing methods [5-9] and the development of engineering guidelines [10-12] to mitigate the risks associated with such constructions. Research studies within FM [13-16] have evaluated the risks associated with traditional cavity wall systems that use aluminum composite material (ACM) or high-pressure laminate (HPL) as claddings. These studies have contributed to the development of the ANSI/FM 4411 standard [17], which employs large-scale fire tests to assess the fire performance of cavity wall systems.

As designers and architects show increasing interest in BIPV façade systems and their usage rises, it becomes crucial to provide corresponding installation, testing, and certification guidelines to properly assess the fire performance of these assemblies under end-use conditions. The objective of this study is to investigate the fire hazards of BIPV façade systems using the large-scale façade fire tests specified in the ANSI/FM 4411 standard. Additionally, PV modules are electrically charged when mounted outdoors as façades, which can increase their temperature. This research also aims to evaluate the effect of PV module charging on the fire performance behavior of wall systems. The findings from this study will contribute to establishing suitable large-scale test methods and guidelines for evaluating the fire performance of these façade systems.

2. BIPV Façades

This section discusses BIPV façades and its components that may contribute to their flammability, the types of BIPV modules prevalent in the construction industry, and the electrical operational stages that affect BIPV module operating temperatures.

2.1 BIPV System and Components

The BIPV façade systems currently available in the market can be broadly categorized into two types. The first type, known as a cavity-wall system, is a popular solution that provides a complete building envelope, as shown in Figs. 1-1(b) and 1-2. The second type, illustrated in Fig. 2-1, is a flexible BIPV system backed by substrates such as insulated metal sandwich panels (IMP), glass curtain walls, or other façades like cladding wall systems. Although both categories of BIPV façades are evaluated in this study, the primary focus is on BIPV cavity-wall systems due to their popularity and wider-spread usage in high-rise buildings.

(a) mounted on an exterior façade

(b) mounted on a cladding wall (photo courtesy of Heliatek)

(c) mounted on IMP backing (photo courtesy of Heliatek)

Figure 2-1: Examples of flexible BIPV facades adhered to various types of mounting substrate.

In a façade system, numerous BIPV modules are electrically wired together to form a "string" of BIPV modules, as depicted in a schematic in Fig. 2-2. The modules are connected in series or in a parallel configuration, and the resultant string is limited by the peak voltage or current of the BIPV system. Each string is then connected to the downstream electrical control system, which is often located in the basement of the building. As illustrated in Fig. 2-2, the downstream system includes an emergency shut-off switch for the DC current, followed by inverters to convert DC to AC, a transformer to adjust the voltage, and ultimately, a choice of an energy storage system or a utility-grid connection, or a hybrid system. The downstream electrical system is also referred to as the AC section [18]. For the purposes of this study, fire hazards associated with the downstream electrical components, which can be sprinkler-protected in a basement, are not considered in this study.

As shown in Fig. 1-2, the PV modules are backed by electrical cables. These cables can be categorized into three types: 1) module cables that connect PV modules via junction boxes; 2) string cables; 3) DC main cables that connect strings to the AC section. Figure 2-2 illustrates the complexity of the cable layout behind the BIPV modules. The string cables have a thicker plastic jacket than module cables, which results in a higher combustible load. The wires are either carried in open trays, as shown in Fig. 2-3(a), or concealed within conduits made of metal or plastic. PV cables may be rated for fire performance in accordance with standards such as UL 4703 [19] or EN 50575 [20]. The junction boxes located behind PV modules, shown in Fig. 2-3(b), contain the electrical components and logic necessary to deliver the current from the PV modules to the string cable lines [21].

In BIPV cavity-wall systems, the modules are mounted on the building's exterior sheathing and insulation using steel or aluminum framing, as illustrated in Fig. 2-4(a). For BIPVs backed by a glass substrate, the aluminum framing is attached to the glass substrate using adhesives, which may be combustible. Flexible BIPVs are generally affixed to the substrate using a peel-and-stick adhesive layer on the back of the BIPV module, as shown in Fig. 2-4(b).

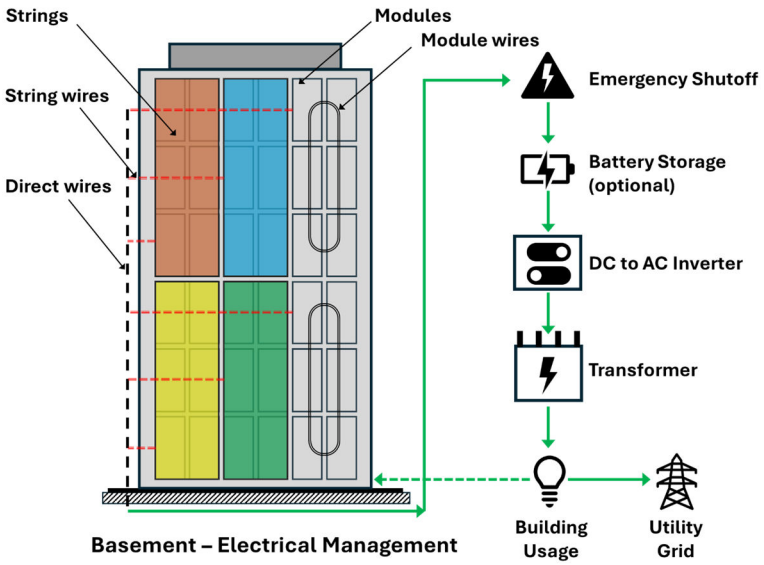

Figure 2-2: A schematic of BIPV installation with façade and downstream electrical components.

(a) open cable trays (photo courtesy of Onyx Solar)

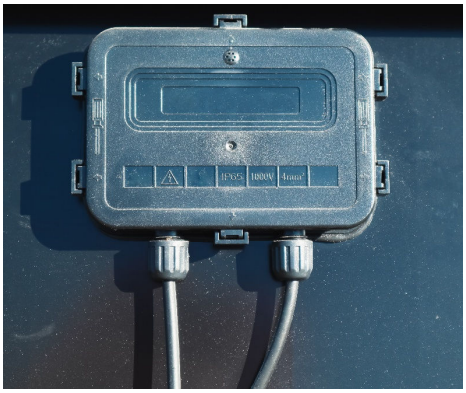

(b) junction box behind module

Figure 2-3: Cables trays and junction boxes used behind BIPV modules.

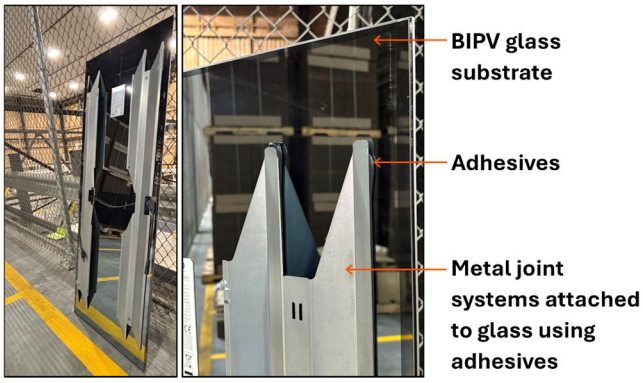

(a) Cavity-wall mounting system for double-sided glass BIPVs

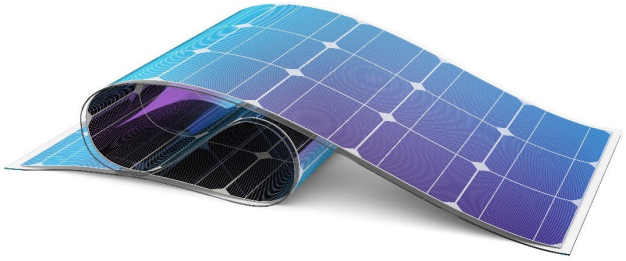

(b) peel-and-stick flexible BIPVs

Figure 2-4: Mounting details of various BIPV façade systems.

The mounting systems for BIPV cavity-wall systems ensure the presence of an air cavity between the PV modules and the insulation backing. The depth of this air cavity can vary from 2 in. to 6 in. (50 mm to 150 mm). The primary function of the air cavity is to allow for rainwater drainage and air ventilation. Unlike traditional cavity-wall systems, the air cavity in BIPV cavity-wall systems contains additional electrical components, such as cables, junction boxes, and inverters, which can be combustible and also ignition sources [18, 22].

2.2 Modules and Solar Cells

The key component of the BIPV cavity-wall system is its PV module cladding. BIPV modules typically consist of a solar cell encapsulated between high-strength tempered glass layers, each approximately 2 to 6 mm thick, which serve as the superstrate and substrate. Thin encapsulant films of plastic sheets, such as ethylene vinyl acetate (EVA) or polyolefin (POE), about 0.2 to 1 mm thick, insulate the solar cell from the glass layers. Modules featuring glass on both sides are referred to as double-sided (bifacial) glass BIPVs. Figure 2-5(a) shows a schematic of the layers in a typical double-sided glass BIPV module.

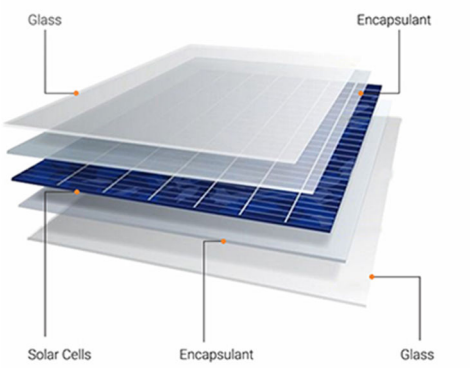

(a) frameless double-sided glass BIPV [23]

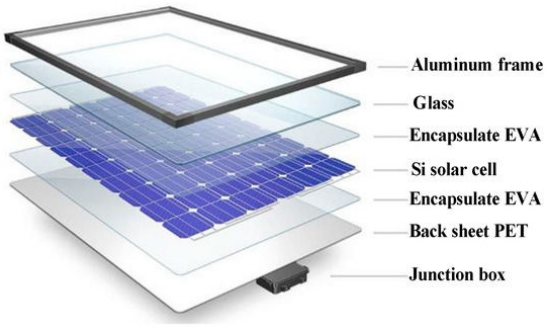

(b) single-sided glass BIPV with metal frame [24]

Figure 2-5: Layers of a typical double-sided glass BIPV module.

Other types of BIPV modules may have plastic back sheets and are referred to as single-side glass BIPVs. The attachment system of some BIPV modules may require metal or plastic framing around the module perimeter, which is bonded to the glass superstrate layer by high-strength adhesives (e.g., polybutyl or silicone). Figure 2-5(b) shows an example of a single-sided glass BIPV with an aluminum frame. In contrast, flexible BIPV panels use a thin flexible polymer sheet, approximately 0.25 to 0.50 mm thick, as both the superstrate and substrate. The key component of the module is its photovoltaic (or solar) cells, which generate electric current. Table 2-1 lists the most popular cell technologies along with their key characteristics.

Table 2-1: Photovoltaic solar cell technologies and generic characteristics. [25]

Technology	Market share	Efficiency	Cost of production
Single crystal silicon (sc-Si)	Highest	Highest	Low
Multi crystal silicon (mc-Si)		High	
Thin film (transparent) • Amorphous Si (a-Si) • Micromorphous Si (μ-Si) CdTe, CIGS, CIS, GaAs, CzTs	Mid	Mid	High
Organic PV (OPV) and others	Low	Low	Low
CdTe: Cadmium telluride CIGS: Copper-indium-gallium-diselenide CIS: Copper-indium-selenide GaAs: Gallium-Arsenide CzTs: Copper-zinc-tin-sulfide			

Out of the various cell technologies available in the market, the most prevalent ones with the highest efficiency and lowest production costs are the wafer-based crystalline silicon (c-Si) cells [25, 26]. The c-Si cells are subdivided into single-crystal silicon (sc-Si) and multi-crystalline silicon (mc-Si) cell technologies, with the former inherently demonstrating higher efficiency (~20-25%) in comparison to the latter (~18-21%) [25]. The other popular category of solar cells is the thin-film cells, which can be made from various semiconductors as listed in Table 2-1 [27]. Thin-film PVs are formed by depositing thin layers of semiconductors onto substrates, thus eliminating the need for an encapsulant under the substrate layer [25]. Typically, the efficiency of thin-film cells is lower, and the production costs are higher than the c-Si counterparts [25, 26]. Lastly, organic PVs (OPVs) use organic material cells, which have lower production costs but also exhibit lower efficiencies [25].

2.3 Electrical Operational Stages

As power-generating devices, the field operational conditions of PV modules differ from those of nonelectrical claddings such as ACMs and HPLs. To define their standard operational conditions, PV modules are tested under 1 kW/m^2 of irradiance, simulating standard test conditions [28]. Under these conditions, a voltage-current (V-I) curve is plotted, as shown in the representative plot in Fig. 2-6(a). The V-I curve delineates the electrical conditions for three important operational stages of PV modules under field conditions, as illustrated schematically in Figs. 2-6(b-d). These stages are briefly described below and significantly influence the temperature boundary conditions of the modules, which are discussed in detail in Section 5.

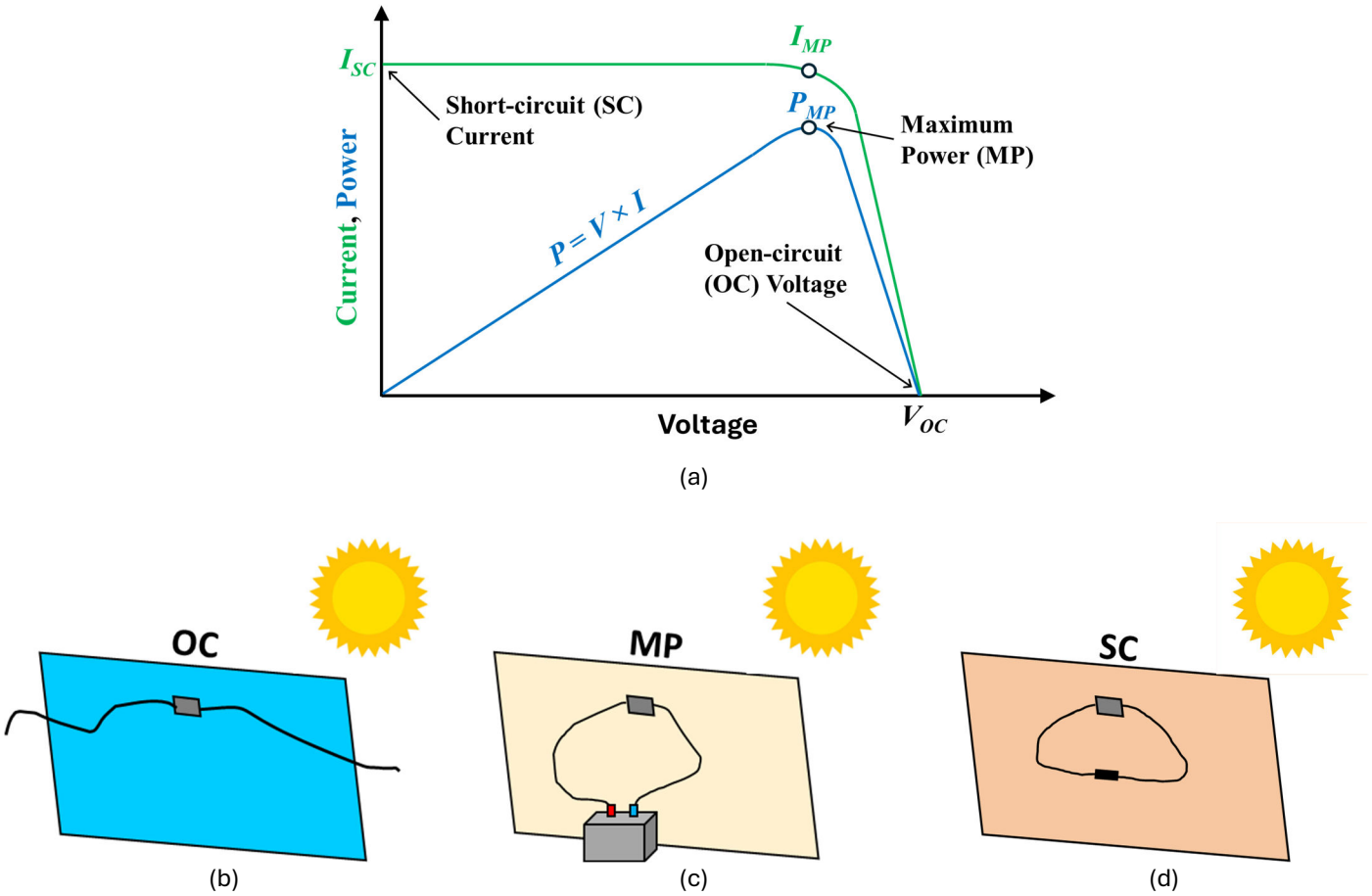

Figure 2-6: (a) A schematic of V-I plot for a photovoltaic cell, demonstrating its operational stages, (b) open-circuit, (c) maximum-power, and (d) short-circuit (SC) schematics.

(i) Open-circuit (OC): In this condition, the solar module generates its maximum voltage (V_{OC}) while the module's wires are left open (i.e., no load is connected). This situation is similar to traditional nonelectrical claddings, such as ACMs or HPLs, installed on buildings, which heat up due to solar heating while absorbing solar irradiance.

(ii) Maximum-power (MP): The maximum power, P_{MP} (= $V_{MP} \times I_{MP}$), is generated under standard test condition of 1 kW/m^2 solar irradiance. This represents the normal operating condition of a solar module, where its surface temperature increases due to solar heating and Joule heating ($= I_{MP}^2 \cdot R$).

(iii) Short-circuit (SC): Maximum current (I_{SC}) flows out of the panel when the positive and negative terminals are short-circuited. Although this is not within the normal operating regime of PV modules, there have been incidences of short-circuit fires caused by faulty electrical components, their weatherization, or improper installations [18, 22]. The temperature of the module under SC conditions is higher than under MP conditions due to the higher current ($I_{SC} > I_{MP}$) passing through its solar cells.

3. International Tests and Research Approach

BIPV products, including those for façades, roofs, and skylights, must meet regulatory approvals for both building material and electrical safety according to local codes. Building material safety standards, particularly fire safety, are derived from UL, ISO, ASTM, NFPA, ANSI, and EN, among others. Electrical safety standards are primarily sourced from IEC or NEC codes. A comprehensive review of these requirements in various countries is available in the literature [29, 30]. This section provides a brief overview of existing fire testing standards, and the research approach used in this work.

The IEC 61730-1 [31] and IEC 61730-2 [32] standards are the primary international guidelines for electrical and mechanical safety requirements of PV/BIPV modules. While these standards do not mandate fire testing, their informative annex references several relevant test methods, including UL 1703 [33] (or ANSI/UL 1703), EN 13501-1 [34] and CEN/TS 1187 [35] test standards. The UL 61730 standards closely align with IEC 61730 requirements, with the addition that UL 61730 mandates compliance with UL 1703 fire test. The EN IEC 61730 adapts the IEC 61730 standards for European regulations but does not include any modifications to fire testing requirements.

UL 1703 is based on the ASTM E108/UL 790 [36, 37] test standards, which primarily evaluate the surface flame spread hazard for roof coverings. However, UL 1703 modifies the test approach for PV roof cover installations. As shown in Fig. 3-1(a), ASTM E108 tests sloped roof decks with dimensions of 4 ft x 8 ft (1.2 m x 2.4 m) under 17.6 ft/s (5.4 m/s) wind-driven flames. The ratings are based on the exposure flame size and the flame spread distance on the roof cover. Unlike ASTM E108, the UL 1703 test as shown in Fig. 3-1(b) uses a minimum separation distance of 36 in. (0.91 m) between the leading edge of the roof deck (exposed to flames) and the leading edge of the PV cover. This configuration does not simulate the worst-case scenario for PV roof covers [38]. Although UL 1703 does not fully address BIPV façade fire scenarios, it remains as a commonly referenced fire test requirement in jurisdictions such as the United States, Australia, Canada, China, and several Asia-Pacific countries such as Japan, Korea, and Singapore [39].

(a) ASTM E108 - roof covers (photo shows the exposure fire to 4 ft long gypsum board)

(b) UL 1703 combustible roof-deck with PV panels at separation distance (photo courtesy of QAI Laboratories)

(c) EN 13501-1 (photographs courtesy of fire testing technology Ltd., FTT)

(d) CEN/TS 1187 Test #3 (photo courtesy of NETZSCH instruments)

Figure 3-1: International tests used for roof and BIPV façade module evaluation.

There are no harmonized BIPV façade testing standards in Europe, and the requirements vary by country. Many countries within Europe use the EN 13501-1 [34] series of test standards for the classification of BIPV as a building material for fire safety, along with the CEN/TS 1187 [35] roof tests. Certain jurisdictions may also use their own country-specific façade fire tests for BIPV evaluation [39]. The EN 13501-1 standard provides a list of bench-scale and intermediate-scale tests used to classify BIPV modules for fire, smoke, and debris. These include ISO 1182 [40] (non-combustibility test using a 750 °C furnace), ISO 1716 [41] (bomb calorimeter), ISO 11925-2 [42] (ignitability from direct flame impingement), and EN 13823 [43] (single burning item). FM datasheet (DS) 1-4 [44] provides a comprehensive summary of individual tests and the classification determination per EN 13501-1. Figure 3-1(c) illustrates the test setups. Similar to UL 1703, CEN/TS 1187 is a sloped roof test used for assessing BIPV façades. Shown in Fig. 3-1(d), this test uses a low-exposure radiant heat flux of 12.5 kW/m^2, along with a wind speed of 9.8 ft/s (3 m/s). During the test, fire spread is measured for damage evaluation, and the classification rating is determined per EN 13501-5 [45]. The fire scenario in this test is considered less severe than that used in the UL 1703 test and is not deemed appropriate for BIPV façade applications.

The test standards adopted by international codes are designed for classification of generic building materials using bench-scale tests, or are adapted from roof PV fire tests that do not accurately represent the severities of a façade fire scenario [16, 46]. As described in Section 2, modern BIPV façades are complex constructions and, therefore, it is crucial to investigate their fire hazards using façade fire testing methods.

The façade fire testing methods, discussed in detail in the literature [46], provide a comprehensive examination of fire hazards by simulating full-scale façade geometries that reflect their representative installation practices. These tests expose the façades to realistic fire scenarios, such as room flashover or exterior fires, enabling an accurate assessment of the potential fire hazards associated with BIPV façades. Such comprehensive testing is essential to ensure that all aspects of fire safety are adequately addressed in these complex systems.

With BIPV façade systems being a relatively new addition to the construction industry, their façade fire testing literature is limited. A recent study [47] conducted a large-scale BIPV façade fire experiment with uncharged modules using the SP-105 [48] standard. The BIPV module in this study consisted of a glass superstrate and a plastic substrate. Shown in Fig. 3-2(a), a 13 ft wide x 20 ft high (4 m x 6 m) single-face façade, with no corner, was constructed with BIPV cladding and gypsum backing. The maximum and minimum air cavity gaps in the system were 2.6 in. (65 mm) and 0.9 in. (23 mm), respectively. The module cables were not interconnected and were coiled inside the attachment frame. The initial fire source was a 60-liter heptane pool fire located in the fire room behind the façade. The room experienced flashover at the base of the façade approximately 15 minutes after the ignition. The failure criteria for the test were based on flame spread distance, heat flux at window openings, and debris [46, 48].

(a) initial setup (b) fire test pictures at various instants from $t \sim 15$ min to $t \sim 30$ min

Figure 3-2: SP-105 fire test for a BIPV façade setup [47]. (Photographs courtesy of RISE Fire Research)

Shown in Fig. 3-2(b), the test resulted in cavity fire propagation to the top of the setup at approximately 30 minutes from ignition and a high amount of falling debris as the main observations. These insights into BIPV façade fire dynamics highlight the limitations of unrepresentative bench-cale and sloped roof tests in accurately assessing the fire performance of BIPV systems. The study underscored the importance of conducting large-scale façade tests to evaluate the performance of BIPV systems. Large-scale façade tests provide a more realistic assessment of fire hazards by capturing the unique characteristics and installation practices of BIPV façades, which cannot be adequately simulated by smaller-scale or roof-based testing methodologies.

The approach employed in this research involves conducting large-scale BIPV façade fire tests to understand the behavior of various systems. The focus is to simulate realistic installations and fire scenarios. For this purpose, the fire testing methods of ANSI/FM 4411 [17], specifically used for evaluating traditional cavity wall constructions, were selected. The two large-scale tests outlined in ANSI/FM 4411 are the 16-ft high parallel panel test (16-ft PPT) and the 8-ft high cavity wall test (8-ft CWT) methods. The 16-ft PPT simulates a severe exterior corner or window flashover fire scenario attacking the façade [13, 14], whereas the 8-ft CWT simulates a fire originating within the cavity of the ventilated BIPV façade system [49]. BIPV façade setups were constructed to reflect realistic installation practices, including interconnecting cables to form electrical series of panels and assessing the effect of module charging on fire performance. Additionally, the effect of module charging on the BIPV module's operational temperature boundary condition was investigated to gain a better understanding of its implications. These configurations are considered essential for gaining insights into the fire dynamics of BIPV façades under realistic conditions, ultimately enabling a more accurate evaluation of the fire performance and safety of BIPV systems in practical building applications.

4. Materials

Five BIPV façade systems were acquired from various manufacturers. The modules differed in aspects such as superstrate and substrate thickness, module size, solar cell technology, encapsulant type and thickness, maximum power rating, among others. Table 4-1 lists the details of all BIPV modules considered: the four cavity-wall modules are identified using Greek symbols to anonymize the manufacturer, followed by the thickness of their superstrate glass. Fig. 4-1 shows photographs of their cut-outs (3.75 in. or 100 mm, in diameter) where the layered cross section can be better appreciated. The cutout of γ–6mm PV was unavailable.

Table 4-1: BIPV products and details.

Name and Tech	Module Size ft x ft [m x m]	Thickness (mm)	Encapsulant and Thickness (mm)	Module and [Encapsulant] mass (kg)	Max power and density*	Fire testing certifications
α–4mm (sc-Si)	5.2 x 2.3 [1.6 x 0.7]	Total: 9 Glass Superstrate: 3.9 Glass Substrate: 3.9	POE, PET, PE, PPE Superstrate: 0.6Δ Substrate: 0.6Δ	25 [1.2]^	195 W 184 W/m²	DIN EN13501-1: B-s1, d0
β–3mm (CIGS)	5.2 x 2.2 [1.6 x 0.7]	Total: 5.5 Glass Superstrate: 3 Glass Substrate: 2.1	POE Superstrate: 0.2Δ Substrate: 0	17 [0.2]^	145 W 137 W/m²	UL 790: Class C DIN EN13501-1: B-s2, d0
γ–4mm (sc-Si)	5.6 x 3.3 [1.7 x 1.0]	Total: 9.8 Glass Superstrate: 4 Glass Substrate: 4	EVA Superstrate: 0.9 Substrate: 0.9	34 [2.8]^	295 W 172 W/m²	UL 1703 passed EN 13501-1
γ–6mm (sc-Si)	5.6 x 3.3 [1.7 x 1.0]	Total: 13.8 Glass Superstrate: 6 Glass Substrate: 6	EVA Superstrate: 0.9 Substrate: 0.9	51 [2.8]^	295 W 172 W/m²	UL 1703 passed EN 13501-1
FlexPV (CIGS)	8.5 x 3.2 [2.6 x 1.0]	Total: 1 PET Superstrate: 0.4 PET Substrate: 0.4	TPO Superstrate: 0.2 Substrate: 0	5.3 [0.5]^ + [3.0]*	340 W 135 W/m²	UL 1703: Class A

sc-Si: single-crystal silicon | CIGS: Copper-indium-gallium-diselenide | mc-Si: multi-crystalline silicon
POE: Polyolefin | PET: Polyethylene terephthalate | PE: Polyethylene | PPE: Polyphenylene ether | EVA: Ethylene vinyl acetate | ETFE: Ethylene Tetrafluoroethylene | TPO: Thermoplastic POE.
Δ Calculated by differences of measurements from product data sheet and lab measurements
^Encapsulant mass estimated based on thickness and an average encapsulant density of 920 kg/m³ [50].
* Includes the mass of PET superstrate and substrate using PET density of 1450 kg/m³ [51].

Four of these modules — α–4mm, β–3mm, γ–4mm and γ–6mm — are meant for cavity wall constructions. The superstrate and substrate of these products are made of high-strength tempered glass. Out of the four BIPV cavity-wall products, the α-4mm, γ–4mm, and γ–6mm modules used the mc-Si technology and have comparable MP density, see Table 4-1. The mc-Si technology requires encapsulants on both the substrate and superstrate. The encapsulant in both γ–4mm and γ–6mm modules is based on EVA, while the α–4mm modules use an encapsulant composed of several polymers, with POE as the major constituent. The encapsulant thickness in both γ–4mm and γ–6mm modules (0.9 mm) is approximately 50% greater than in the α–4mm modules (0.6 mm).

FlexPV is the only self-adhering flexible BIPV module obtained for this work. The module has a thin plastic superstrate and substrate, as detailed in Table 4-1. The substrate side consists of a high-strength polyvinyl acetate (PVA) adhesive layer that is 0.76 mm thick and protected by a peel-off skin cover. The junction box and cables for the FlexPV module are adhered to its edge, as shown in Fig. 2-4(b).

(a) α–4mm

(b) β–3mm

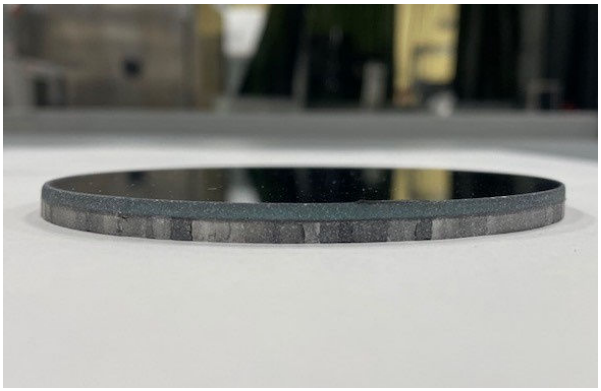

(c) γ–4mm

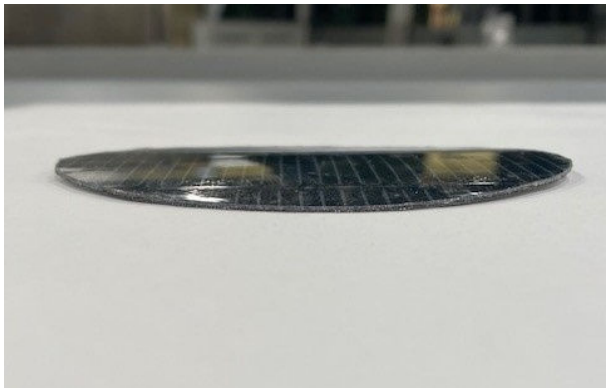

(d) FlexPV

Figure 4-1: Photographs of the cut-outs of four BIPV modules showing their multiple layers. The superstrate side is facing upward. Cracks on glass are from the machining process.

The β–3mm and FlexPV modules use "thin film" CIGS solar cell technology, in which solar cells are directly etched onto the substrate layer. As a result, no encapsulant is present on the substrate side. β–3mm uses a POE encapsulant, while FlexPV uses a thermoplastic POE (TPO) polymer encapsulant. The superstrate encapsulant thickness for both modules is 0.2 mm. As mentioned in Section 2.2, the thin-film modules exhibit a lower maximum power density than the mc-Si counterparts.

Comparing the four BIPV cavity-wall products, the α–4mm and γ–4mm modules use approximately 4 mm for both the superstrate and substrate layers. The β–3mm modules use relatively thinner glass layers—3 mm for the superstrate and 2 mm for the substrate. The γ–6mm modules are similar to the γ–4mm modules, except for a higher glass thickness of 6 mm each on both superstrate and substrate ends. FlexPV modules, on the other hand, consist of significantly thinner layers of about 0.4 mm for both the superstrate and substrate, primarily made of PET (polyethylene terephthalate) polymer, making them significantly lighter than their cavity-wall counterparts.

The mounting systems for all four products came factory-installed on their glass substrates. The α–4mm and β–3mm modules have steel mounting systems, while the γ–4mm and γ–6mm modules have aluminum mounting systems. The mounting system for γ–4mm and γ–6mm modules differed with each other, and these details will be discussed in Section 6. The junction box and power cables came attached with the modules on their substrates. Figure 2-4(a) shows back side and attachment detail of an α–4mm BIPV module.

In terms of fire testing certifications, the modules have been evaluated against the sloped roof tests (UL 1703/UL 790) and the EN 13501-1 series of tests. The test methods and their shortcomings were discussed previously in Section 3. The test reports were not made available for review.

5. Measurement of BIPV Operational Temperatures

5.1 Setup and Test Matrix

The modules were first evaluated for their operational temperature boundary conditions using a series of outdoor and indoor tests. Operational temperature data were not collected for the γ–6mm modules. Figure 5-1 shows pictures of the two setups, and Table 5-1 presents the test matrix.

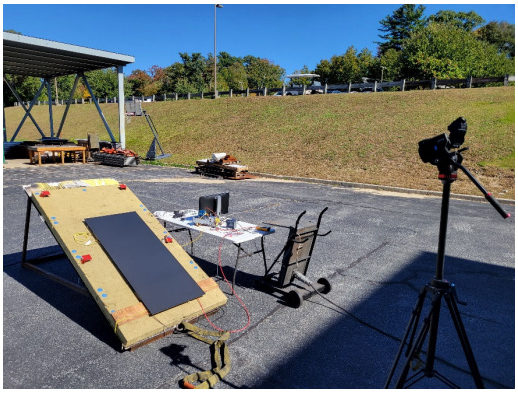

(a) outdoor test setup

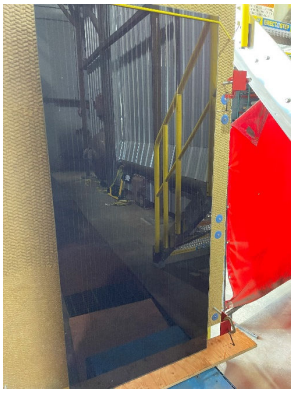

(b) indoor test setup

Figure 5-1: Setup pictures for PV operational temperature measurements.

Table 5-1: Test matrix for the PV operational temperature measurements.

Module name	Outdoor				Indoor			
	OC	MP	SC	OC	1xMP	1.5×MP	2×MP	SC
α–4mm	✓	✓	✓	✓	✓	✓	✓	✓
β–3mm	✓	NA	✓	✓	NA	NA	NA	✓
γ–4mm	✓	C	✓	✓	✓	X	✓	✓
γ–6mm	X	X	X	X	X	X	X	X
FlexPV	✓	✓	✓	✓	✓	✓	✓	✓
NA – β–3mm modules cannot be charged with reverse current from an external power supply. C – Datafile corrupted. X – No data taken for γ–6mm module.								

The outdoor tests were conducted during the summer months. The modules were mounted on a metal frame, inclined approximately 30 degrees from the horizontal, and backed by 2 in. (50 mm) of mineral wool (MW) insulation with 2 in. (50 mm) air cavity spacing to simulate a cavity-wall setup. A Schmidt-Boelter radiometer with a range of 0 to 2 kW/m^2 was used to measure the irradiation received from the sun towards the modules. The test data was collected when the irradiation was steady at 1 ± 0.1 kW/m^2 for approximately 15-minute period. The instrumentation included an infrared (IR) camera – FLIR A655sc, –40°F to 302°F (–40°C to 150°C) range, accuracy maximum of ± 3.6°F (± 2°C) or ± 2 % of reading – to measure the superstrate temperature. However, due to the wide spectral range (~7-14 μm) of the IR camera and the regions of low emissivity of glass in that wavelength range, an effective lumped temperature of superstrate glass, encapsulant, and solar cell is measured [52]. Furthermore, because the reflections from the glass superstrate are specular in nature [53], the IR camera temperature data can only be used for qualitative comparisons. The temperatures of the substrate layer, the insulation behind the module, and its cabling were measured using an IR gun thermometer. The temperature data of the modules was collected under OC, MP, and SC conditions.

For the indoor tests, the modules were mounted vertically on a metal frame with the same insulation backing as in the outdoor tests and were not exposed to any solar irradiation. The instrumentation remained consistent with the outdoor tests. The electrical operational conditions used were OC, 1× MP, 1.5× MP, 2× MP, and SC, as shown in Table 5-1. The MP charged conditions required external power supplies (AIM-TTI QPX600DP, with a maximum power rating of 80 V, 50 A, and 1.2 kW) to provide reverse-flow current to the modules at various factors of its maximum rated voltage and current.

During both outdoor and indoor tests, the β–3mm modules could not be operated under the MP conditions due to its junction box electrical logic prohibiting any reverse current flow.

5.2 Results and Discussion

Figure 5-2 shows the IR images of an α–4mm module during outdoor tests — the temperature profiles during OC, MP, and SC operational stages are shown. Similar IR profiles of outdoor tests for other modules are provided in Appendix A.

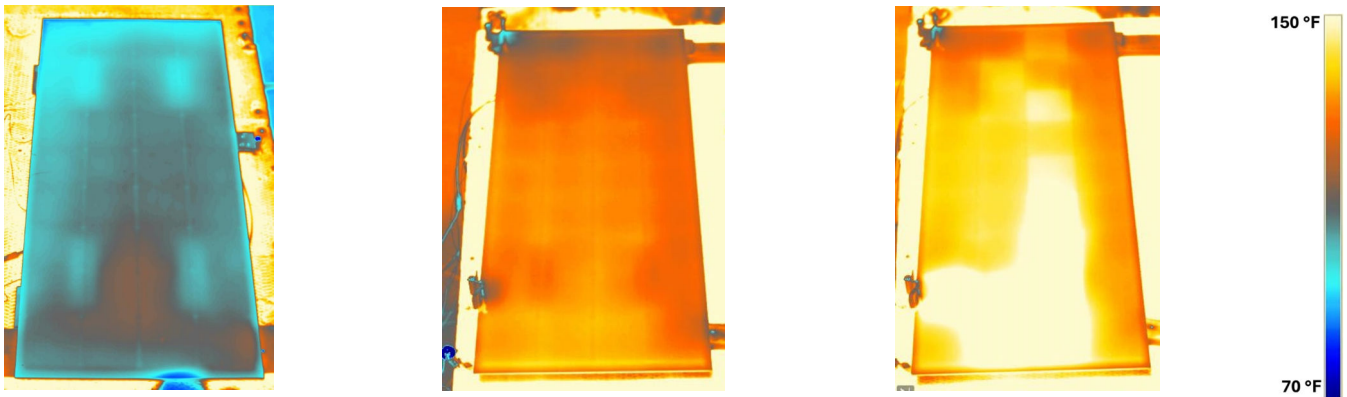

(a) OC: 120°F (49°C) (b) MP: 144°F (62°C) (c) SC: 196°F (91°C)

Figure 5-2: Temperature profiles and maximum temperature of α–4mm modules during outdoor tests at various operational stages.

Figure 5-2(a) shows the temperature profile under the open-circuit (OC) condition, where there is no power load, and the temperature rise of the module is solely due to heating from solar irradiance (~ 1 kW/m^2). In the maximum power (MP) condition, depicted in Fig. 5-2(b), additional heat transfer occurs due to the Joule heating effect ($= I_{MP}^2 \cdot R$), which further increases the module temperature. Lastly, during the short-circuit (SC) condition, several cells within the module undergo a short circuit and exhibit higher temperatures due to a higher current ($I_{SC} > I_{MP}$) passing through the solar cells.

It is noted that PV fire testing, and in particular, façade fire testing, is conducted indoors inside a controlled atmosphere lab space. Correspondingly, the indoor test results for α–4mm modules in various charged-up states are shown in Fig. 5-3. Indoor testing profiles of other modules are presented in Appendix A.

At the 1×MP condition shown in Fig. 5-3(a), the module temperature of 104 °F is lower than the 144 °F observed in outdoor tests in Fig. 5-2(a). This difference is attributed to the heating effect of solar irradiance (~1 kW/m^2) in the outdoor tests. To replicate 1×MP outdoor conditions indoors, the modules would need to operate at 2×MP conditions, as shown in Fig. 5-3(c), where the temperature reaches 136°F (58°C). However, forcing a reverse current that is twice the maximum rated current into a module is not feasible, as the junction box logic for many modules may prevent overcharging of solar cells.

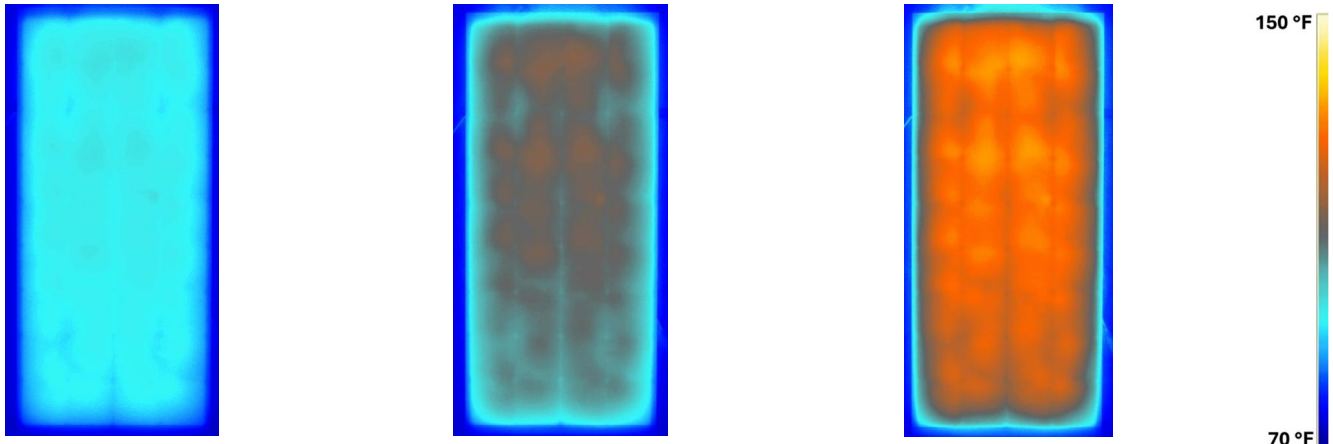

(a) 1×MP: 104°F (40°C) (b) 1.5×MP: 119°F (48°C) (c) 2×MP: 136°F (58°C)

Figure 5-3: Temperature profiles and maximum temperature of α–4mm modules during indoor tests at various power settings.

One consequence of a module heating up under 1×MP conditions is the increased temperature of the plastic encapsulants. Figure 5-4 illustrates the phase change behavior of EVA encapsulants, as compiled from the literature [54]. Phase change behavior of POEs is similar and is reported in the literature [55, 56].

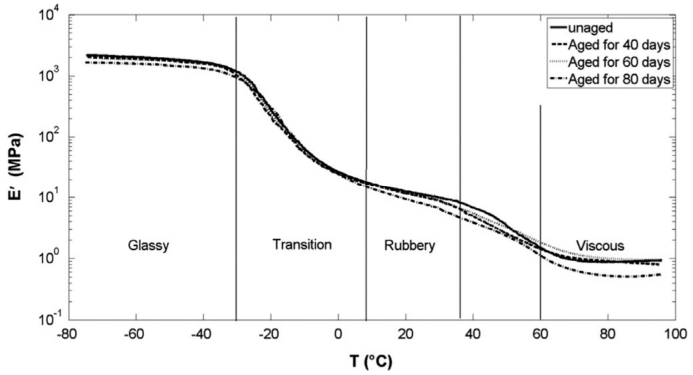

Figure 5-4: Storage modulus of EVA encapsulant during thermal degradation from literature [54].

The operating temperature range of EVA within a solar module is typically -40°F to 185°F (-40°C to 85°C); however, under realistic conditions, the temperature can reach as high as 212°F (100°C) [57-59]. Within this temperature range, EVA, being a viscoelastic material, can exist in different stages — glass, rubberized, or viscous — depending on the temperature, as shown in Fig. 5-4. The melting point of EVA, where it transitions to a viscous stage, occurs between 104°F and 140°F (40°C and 60°C), which is well within its operational range. The differential scanning calorimetry analysis from Reference [57] shows that the melting point of EVA used in PVs is approximately 113°F (45°C), as evidenced by an endothermic enthalpy of melting peak.

Lastly, operating at 1×MP condition also heats up other flammable components of the system, such as electrical cables and the insulation backing of the module. The temperature of these parts rises to levels comparable to the temperatures measured for the superstrate of the modules. Appendix A provides additional data on insulation and cable temperatures.

The results indicate that the fire performance of BIPV systems should be evaluated under both uncharged and charged conditions to better understand its impact on the overall flammability of the system. PV modules operating under MP conditions represent a more realistic scenario before a fire occurs. Testing under OC conditions is also needed, as it represents the state when the PV system is uncharged and provides insights into the baseline thermal characteristics and fire responses of the system without electrical influence.

During the ANSI/FM 4411 fire tests, modules operating under SC conditions were not considered. While there have been recorded fire incidents in PV systems originating due to short circuits [18], the likelihood of a significant façade fire scenario occurring simultaneously with the module operating in SC condition is relatively low. Therefore, the ANSI/FM 4411 fire tests focus exclusively on OC and MP conditions, as these conditions provide a more representative understanding of the typical states PV modules experience. This structured testing approach ensures a comprehensive assessment of the BIPV system's fire performance in the most critical and probable operational scenarios.

6. FM 4411 Setups and Test Matrix

6.1 16-ft PPT BIPV Tests

The 16-ft PPT of ISO 3957 [60] is the primary test method of ANSI/FM 4411, which simulate fire scenarios such as exterior and flashover fires. The setup consists of two identical façade systems, each 16 ft (4.9 m) high and 3.5 ft (1.1 m) wide, mounted parallel to each other with a 1.75 ft (0.5 m) separation. A 360-kW propane sand burner provides a peak heat flux of approximately 100 kW/m^2 to the lower portions of both façades for the 15-minute test duration. The setup is placed under a 5 MW calorimeter to measure the heat release rate (HRR), which correlates with flame spread extent and the fire propagation propensity of the wall systems [14, 16]. Based on this principle and the risk criteria of the FM corner fire tests [13, 14, 61, 62], two peak HRR thresholds are used to evaluate the fire performance of a cavity wall system [16, 17, 60]: (1) for unlimited height approval of a wall assembly, peak HRR must not be greater than 830 kW; and (2) for 50 ft (15.2 m) height approval, peak HRR must not be greater than 1100 kW. Wall systems with a peak HRR higher than 1100 kW are deemed unacceptable.

The BIPV cavity wall systems were prepared as shown in Fig. 6-1, using α–4mm BIPV as an example. First, the two metal frames, each 16 ft high and 3.5 ft wide (4.9 m x 1.1 m), were covered with ½ in. (13 mm) thick fire-retardant plywood and 5/8 in. (16 mm) thick non-combustible Type-X gypsum boards as the exterior sheathing. A two-inch (50 mm) thick layer of non-combustible mineral wool (MW) insulation was then mounted as backing, as shown in Fig. 6-1(a). The BIPV modules were attached on top of the MW insulation using manufacturer-provided systems (Fig. 6-1b), creating an approximate cavity depth of 4 in. to 4.75 in. (100 mm to 120 mm) (Fig. 6-1c). The modules were arranged with centrally located vertical joints, and the perimeters of the assemblies were further covered with 16-gauge steel sheets. In comparison, the FlexPV modules were directly adhered to the non-combustible gypsum exterior sheathing using the manufacturer's peel-up adhesive. The two identical wall systems were mounted facing each other in a parallel configuration on a weighing platform to continuously record mass loss data during the test, as shown in Fig. 6-1(d). The HRR and mass loss data were smoothed using a Savitzky-Golay filter [63-65]. Detailed preparation procedures for other BIPV wall systems are provided in Appendix B.

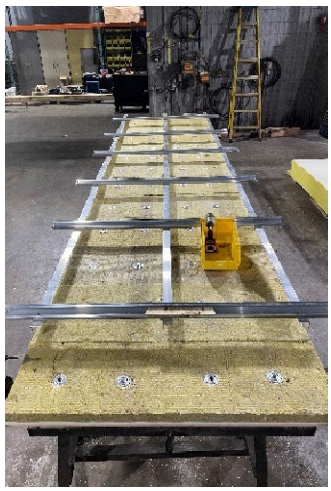

(a) attachment system atop MW and gypsum

(b) PV module attached using mounting system

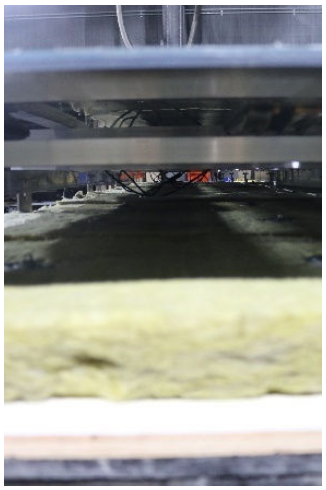

(c) Open cavity feature of α–4mm system

(d) Complete assembly with the charging setup

Figure 6-1: 16-ft PPT setup preparation for α–4mm cavity-wall façade setup.

The attachment system details for BIPV cavity wall systems differed from one another. Some relevant attachment system details for β–3mm , γ–4mm, and γ–6mm modules are shown in Fig. 6-2. The attachment systems of α–4mm and β–3mm modules result in an open air cavity of 4 in. to 4.75 in. (100 mm to 120 mm) depth, as observed in Figs. 6-1(c) and 6-2(a), respectively. The attachment system of the γ–4mm modules, shown in Fig. 6-2(b), includes horizontal joints located approximately every 2 ft (0.6 m), which effectively reduces the air cavity depth from approximately 4 in. (100 mm) to 1.6 in. (41 mm). The γ–6mm module goes a step further by using stiffeners and cleats as cavity restrictors, as shown in Fig. 6-2(c), to

effectively compartmentalize the air cavity into 2 ft sections. The γ–4mm and γ–6mm cavity restrictors are designed to develop passive fire protection that reduces flame passage thickness and thereby flame spread rate within cavities.

(a) β–3mm

(b) γ–4mm

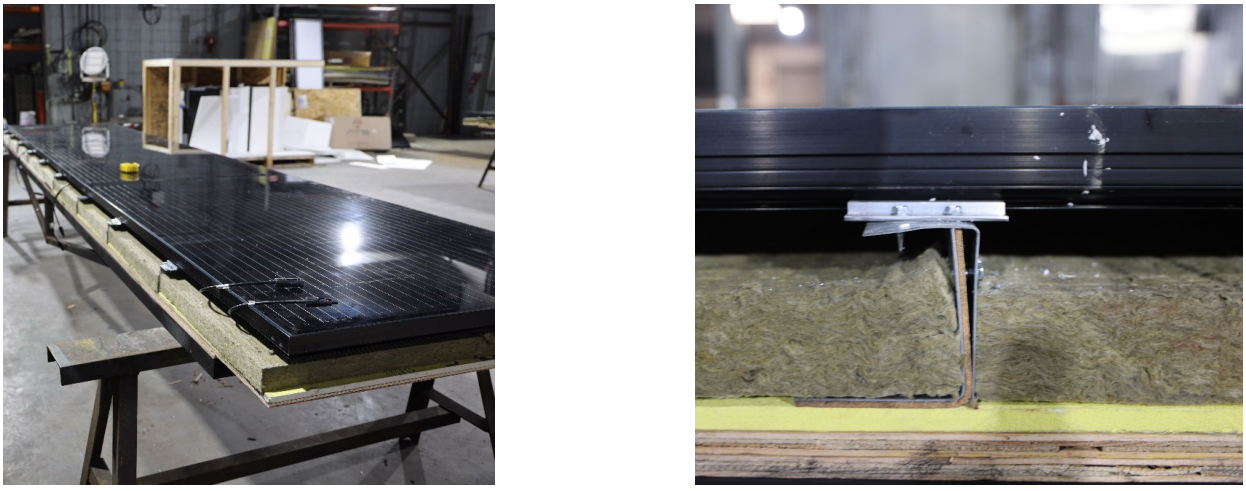

(c) γ–6mm

Figure 6-2: Attachment system details for β–3mm, γ–4mm, and γ–6mm modules

Modules for the 16-ft PPTs were supplied with the standard size stocks available from the manufacturers. Unlike other cladding products, BIPVs cannot be machined to the exact dimensions of the 16-ft PPT setup due to the risk of cracking the tempered glass. Consequently, the final dimensions of the BIPV assemblies slightly differ from the standard 16 ft high and 3.5 ft wide (4.9 m x 1.1 m) dimensions. Figure 6-3 shows the dimensions of each BIPV setup compared to the 16-ft PPT frame, as well as the number of modules used on each side of the metal frame.

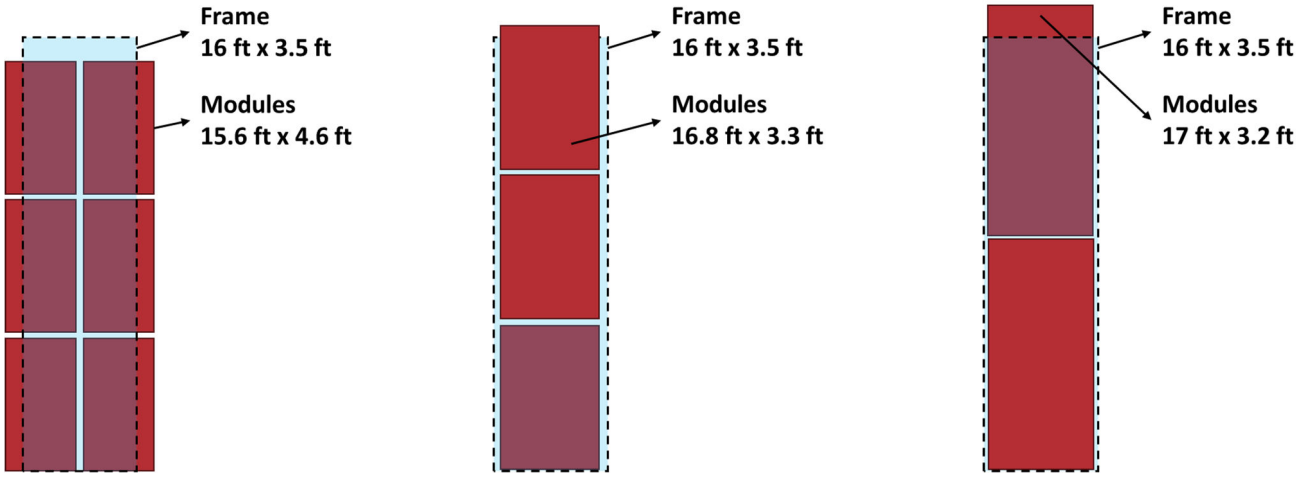

(a) α–4mm and β–3mm (b) γ–4mm and γ–6mm (c) FlexPV

Figure 6-3: Installation configuration, number of modules, and dimensions per 16-ft PPT metal frame.

For the tests conducted under MP-charged conditions, three power supplies (AIM-TTI QPX600DP, with a rating of 80 V, 50 A, and 1.2 kW) were used to provide reverse-flow current to the modules at their maximum-rated voltage and current. Figure 6-1(d) show modules connected to external power supplies during a charged BIPV test. The junction boxes of β–3mm modules prevented reverse current flow; therefore, their charged tests were not conducted. To achieve a steady-state temperature before the tests, the modules tested under MP conditions were charged for a minimum 1 hour prior to ignition.

Table 6-1 provides the 16-ft PPT test matrix and details on the electrical connections between the power supply and the BIPV modules. The initial temperature of the modules in 1×MP tests is consistent with the measurements in Section 5. For the tests conducted under OC conditions, the cables were connected in the same manner as in MP condition tests, but the power supplies were turned OFF.

Apart from the standard HRR and mass loss measurements, additional instrumentation was used for the 16-ft PPTs. Eight cavity thermocouples (CTCs, type K, 28 gauge, unsheathed, ungrounded) were mounted within the air cavity at every 2 ft (0.6 m) height from the base to monitor the cavity flame spread rate. These CTCs were positioned along the vertical central seam of the BIPV modules, exposed 1 in. (25 mm) from the MW insulation layer, and directed towards the substrate side of the BIPV modules. A surface thermocouple (STC, type K, 28 gauge, unsheathed, ungrounded) was adhered to the BIPV superstrate at a height of 15 ft (4.6 m) along the central seam. Additionally, a water-cooled (~60°C or 140°F) total heat flux gauge (HFG, Schmidt-Boelter, range 0-200 kW/m^2, accuracy ±5%, repeatability 0.5%) was mounted at the top of the setup, flush with the BIPV superstrate, to measure the flame heat flux.

For γ–6mm OC (Test #4) and MP tests (Test #8), two HFGs were placed at 8 ft (2.4 m) and 12 ft (3.7 m) heights within the cavity, flushed along the MW insulation and facing the air cavity, to track the cavity fire spread during the tests. For these two tests with γ–6mm modules, the HFG at the top of the setup location was not connected.

Along with the high-definition (HD) video imagery of the tests, two additional cameras were utilized. A bullet HD camera, with a diameter of 1 in. (25 mm), was placed at the top of the 16-ft PPT setup, looking downward within the air cavity of the wall system to monitor the cavity fire growth during the tests.

Table 6-1: 16-ft PPT test matrix and electrical connection details for 1×MP tests.

Test #	Module and Assembly Description	Charged Status [Δ]	Cabling Details[×]
1	α–4mm → 4.75 in. cavity → 2 in. thick MW → Gypsum	OC	• Six modules in each frame connected in series. • Total 2 strings of 6 modules each.
2	β–3mm → 4.125 in. cavity → 2 in. thick MW → Gypsum	OC	• Six modules in each frame connected in parallel. • Total 2 strings of 6 modules each.
3	γ–4mm → 4 in. cavity → 2 in. thick MW → Gypsum	OC	• Three modules in each frame connected in series. • Total 2 strings of 3 modules each.
4	γ–6mm → 4 in. cavity → 2 in. thick MW → Gypsum	OC	• Three modules in each frame connected in series. • Total 2 strings of 3 modules each.
5	FlexPV → Gypsum	OC	• One module connected to power supply. • Total 4 strings of 1 module each.
6	α–4mm → 4.75 in. cavity → 2 in. thick MW → Gypsum	MP	• Six modules in each frame connected in series. • Total 2 strings of 6 modules each.
7	γ–4mm → 4 in. cavity → 2 in. thick MW → Gypsum	MP	• Three modules in each frame connected in series. • Total 2 strings of 3 modules each.
8	γ–6mm → 4 in. cavity → 2 in. thick MW → Gypsum	MP	• Three modules in each frame connected in series. • Total 2 strings of 3 modules each.
9	FlexPV → Gypsum	MP	• One module connected to power supply. • Total 4 strings of 1 module each.

[Δ] OC → Uncharged (power supplies turned OFF) and MP → Charged (power supplies are ON).
[×] Cables for the OC tests were connected in the same manner as MP tests, but the power supplies were turned OFF.

6.2 8-ft CWT BIPV Tests

The 8-ft CWT of ANSI/FM 4411 simulate fires originating within a cavity, such as electrical, welding, and flying ember fires, [49]. The setup comprises two panels, each measuring 8 ft (2.4 m) high and 4 ft (1.2 m) wide, representing a BIPV module and an insulation backing to replicate a wall cavity. Two-inch (50 mm) thick MW insulation backing was used in the tests. The module and the MW insulation are separated by a representative cavity depth which can be either 2 in. (50 mm) or 4 in. (100 mm), according to ANSI/FM 4411. The BIPV cavity wall systems used in this study had a cavity depth of 4 in. to 4.75 in. (100 mm to 120 mm). Therefore, 8-ft CWTs were conducted with a cavity depth of 4 in. (100 mm). Representative photographs of the test setups are shown in Fig. 6-4, and additional details are provided in Appendix B. The 8-ft CWTs were not conducted for γ–6mm BIPVs.


(a) façade side of BIPV

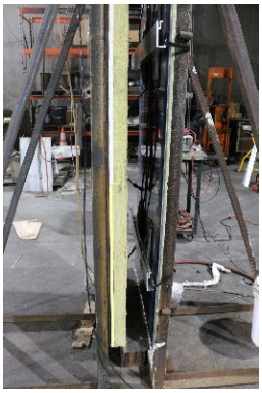
(b) 4 in. cavity and burner


(c) flames at ignition

Figure 6-4: 8-ft CWT setup of α–4mm BIPV wall system in MP condition test

The BIPVs could not be machined to the exact dimensions required for the 8-ft CWT setup. Therefore, the final BIPV assembly dimensions vary from the standard 8 ft high and 4 ft wide (2.4 m x 1.2 m) specifications. Figure 6-5 displays the dimensions of each BIPV setup, as well as the number of modules used.

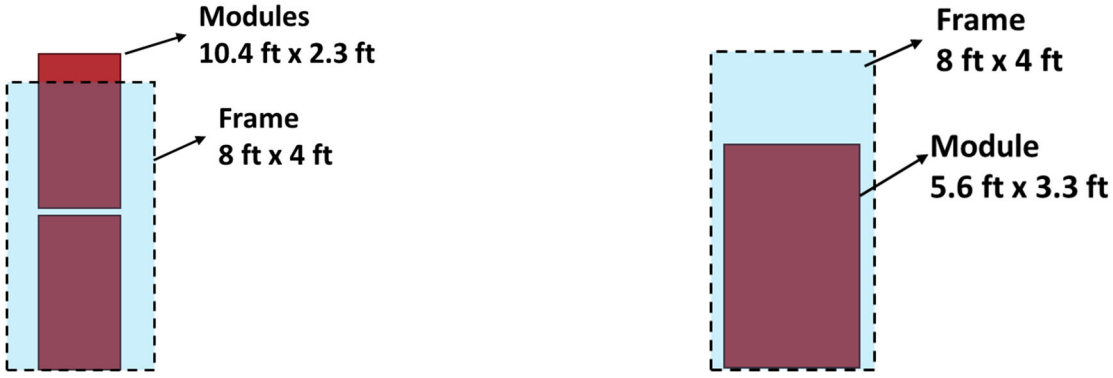

(a) α–4mm and β–3mm (b) γ–4mm

Figure 6-5: Installation configuration, number of modules, and dimensions for 8-ft CWTs.

The setup is placed under a 1-MW calorimeter. For a 4 in. (100 mm) cavity depth scenario, a propane sand burner of 12 in. (305 mm) length and 4 in. (100 mm) depth is used as an ignition fire source. The burner provides approximately 10 kW exposure with a 0.3 m (1 ft) high flame, delivering a peak heat flux of 40 kW/m^2 to the lower portion of the two panels for a 15-minute test duration [49]. HRR and flame height are monitored during the test to evaluate its fire performance. The ANSI/FM 4411 protocol uses an HRR threshold of 100 kW and a flame height threshold of 6 ft (1.8 m) for its pass/fail criteria.

Table 6-2 presents the test matrix for the 8-ft CWTs. Tests for the α–4mm and γ–4mm wall systems were conducted in 1×MP charged conditions, as this scenario was considered more severe compared to the uncharged (OC condition) tests. In contrast, the β–3mm modules were tested in the OC condition since these could not be reverse charged from an external power source.

Table 6-2: 8-ft CWT test matrix and electrical connection details for 1×MP tests.

Test #	Module and assembly description	Charged status [Δ]	Cabling details[×]
10	α–4mm → 4 in. air cavity → 2 in. thick MW	MP	• 2 modules connected in series; 1 String.
11	β–3mm → 4 in. air cavity → 2 in. thick MW	OC	• 2 modules connected in parallel; 1 String
12	γ–4mm → 4 in. air cavity → 2 in. thick MW	MP	• One module connected to power supply.

[Δ] OC → Uncharged (power supplies turned OFF) and MP → Charged (power supplies are ON).

In addition to the HRR measurements under the 1 MW calorimeter hood, flame heights were observed using an HD camera placed in front of the cavity. A water-cooled (approximately 60°C or 140°F) total HFG (Schmidt-Boelter, range 0-200 kW/m^2, accuracy ±5%, repeatability 0.5%) was mounted at a height of 6 ft (1.8 m) flush with the MW insulation and exposed to the cavity. Additionally, a CTC (type K, 28 gauge, unsheathed, ungrounded) was installed within the cavity at the 6 ft (1.8 m) height, along the vertical central seam. The CTC was positioned 1 in. (25 mm) away from the MW insulation layer and directed towards the substrate side of the BIPV module. A STC (type K, 28 gauge, unsheathed, ungrounded) was adhered to the BIPV substrate at the 6 ft (1.8 m) height along the central seam. For the γ–4mm panel tests, the locations of the HFG, CTC, and STC were reduced to a height of 5 ft (1.5 m) due to the decreased height of the setup, as illustrated in Fig. 6-5.

7. Results and Discussion

7.1 16-ft PPT

7.1.1 Uncharged Cavity Wall BIPVs

The section discusses the results of the 16-ft PPT tests for uncharged BIPV cavity wall systems. Figure 7-1 presents the HRR profiles and Fig. 7-2 shows the peak HRR photographs for BIPV cavity wall systems in Tests #1 to #4. Figure 7-3 shows the post-test pictures for Tests #1 to #4. According to the ANSI/FM 4411 standard, an unlimited height installation approval is given for systems with a peak HRR ≤ 830 kW. A 50-ft (15 m) limited height installation approval is granted for systems with a peak HRR ≤ 1100 kW but greater than 830 kW. As observed from Figs. 7-1 and 7-2, all uncharged BIPV systems, except for γ–6mm OC in Test #4, exceeded both peak HRR thresholds, and as a result, the fire propagated to the top of the respective setups. Fire propagation in Test #4 was restricted to 8 ft (2.4 m) height from the base of the setup.

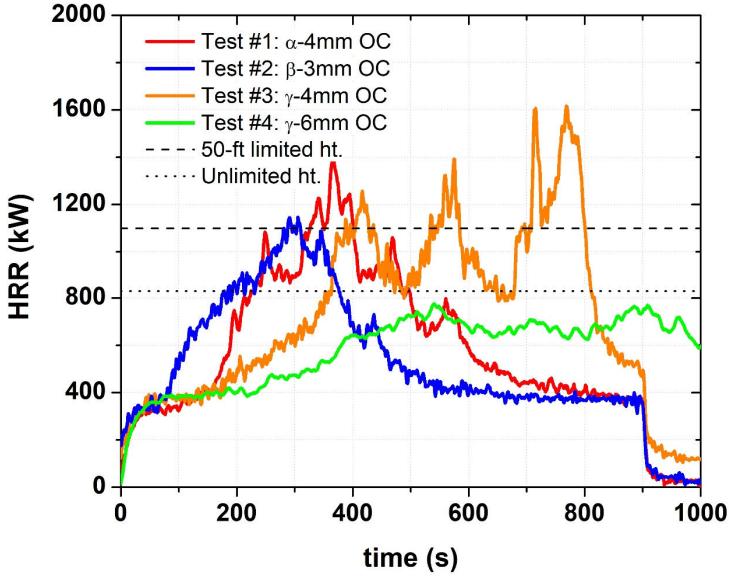

Figure 7-1: HRR profiles for uncharged BIPV cavity wall systems (Tests #1-4).

(a) α–4mm OC: Test #1 (b) β–3mm OC: Test #2 (c) γ–4mm OC: Test #3 (d) γ–6mm OC: Test #4

Figure 7-2: Peak HRR and fire propagation instants of the uncharged BIPV cavity-wall fire tests.

(a) α–4mm OC: Test #1 (b) β–3mm OC: Test #2 (c) γ–4mm OC: Test #3 (d) γ–6mm OC: Test #4

Figure 7-3: Post-test photographs of the uncharged BIPV cavity-wall fire tests.

The primary observations from the fire tests of the BIPV cavity-wall façades made of double-sided glass PVs (Tests #1 to #4) were consistent. Figure 7-4 provides a schematic to explain the sequence of events and facilitate discussion.

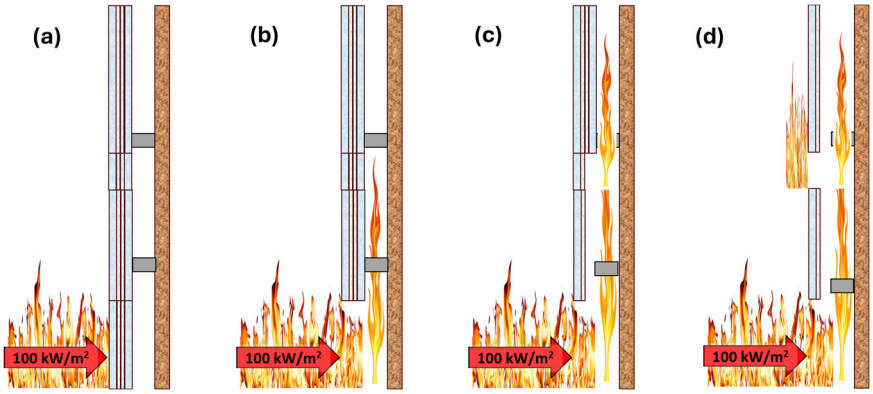

Figure 7-4: Schematic of fire propagation in BIPV cavity wall systems.

(a) Glass shattering: The 360-kW propane ignition provided a peak heat flux of approximately 100 kW/m^2 to the bottom of the BIPV modules (at a height of ~4 ft or 1.2 m). A high temperature gradient along the planar direction of the length of glass modules (~5 ft or 1.5 m) introduces high thermal stress due to glass expansion [66, 67]. Within 1-2 minutes for Tests #1 to #3 and at approximately 5 ½ minutes for Test #4, the front and back glass panels shattered, allowing the propane flames to enter the wall cavity (Figs. 7-4(a) and 7-4(b)).

(b) Cavity propagation: Flames traveled through the 4 to 4.75 in. (100 to 120 mm) deep cavity due to the chimney effect, along the electrical cables to the top of the façade system (Fig. 7-4(c)) in Tests #1 to #3. The cavity flames heated and eventually shattered the substrate-side glass, releasing encapsulant pyrolysates (EVA or POE) that added fuel and further drove the cavity fire growth (Fig. 7-4(c)). In Tests #4, the presence of cavity restrictors that effectively compartmentalized the cavity every 2 ft (1.2 m) restricted the fire growth.

(c) Exterior fire: Due to limited oxygen within the cavity, the flames spills over to the exterior of the façade at the horizontal joint locations, as shown in Fig. 7-2(a) for α–4mm OC (Test #1) and Fig. 7-2(c) for γ–4mm OC (Test #3). This phenomenon from the horizontal joint locations is illustrated in Fig. 7-4(d).

(d) Debris: The cavity fires degraded the adhesives bonding the mounting system to the glass PV panels, causing the PV modules to fall onto the propane fire and shatter. This allowed more oxygen transport into the cavity, leading to enhanced burning and increased HRR, while encapsulant fuel from the shattered panels further fueled the fire, leading to HRR spikes. These phenomena will be discussed in further detail in subsequent sections.

The cavity fires initially drove propagation within the BIPV cavity wall systems. Figure 7-5 shows images captured by the bullet camera located at 16 ft (4.9 m) height within the 4.75 in. (120 mm) deep cavity of the α–4mm OC (Test #1) setup, with the camera filming downwards towards the base of the setup. As mentioned in Section 6.1, although the OC tests were conducted under uncharged conditions, the electrical cables were connected to simulate realistic installations.

(a) Ignition, t = 0 s.

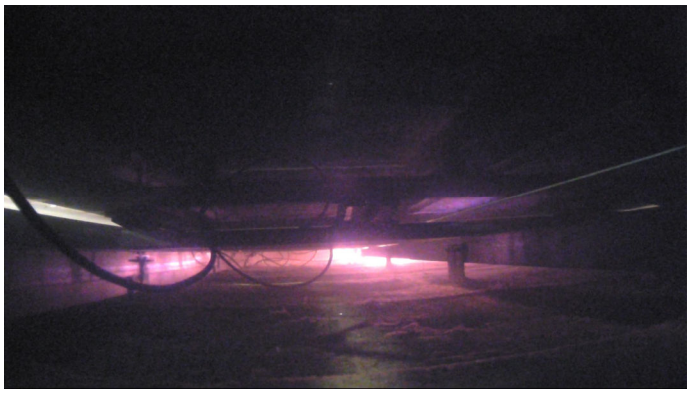

(b) Glass crack and flames inside, t = 3 m 30 s.

(c) cavity fire propagation initiation, t = 3 m 40 s.

(d) cavity fire propagation, t = 3 m 50 s.

(e) cavity fire propagation, t = 4 m.

(f) cavity fire propagation, t = 4 m 15 s.

Figure 7-5: Test #1 (α–4mm OC) test viewed from the cavity bullet camera. The camera is placed at 16-ft height inside the cavity and views downwards towards the burner at the base of the setup.

As observed from Fig. 7-5(a), the bullet camera provides a clear view of the BIPV cavity, with the bottom edge showing the mineral wool insulation and the top edge showing the BIPV substrate. The cables run vertically along the height of the cavity. The open joint systems allow light from the laboratory inside the cavity wall. The snapshots in Fig. 7-5 depict an accelerated cavity fire spread following the shattering of the bottom glass from the approximately 4 ft (1.2 m) tall propane ignition source (Fig. 7-5b). Within approximately 45 s, from Fig. 7-5(b) taken at 3 m 30 s from ignition to Fig. 7-5(f) taken at 4 m 15 s from ignition, the flames travel through the 16 ft (4.9 m) height of the setup along the vertically oriented cables.

Figure 7-6 shows the CTC data for probes located at heights of 4 ft (1.2 m), 8 ft (2.4 m), 10 ft (3.0 m), and 14 ft (4.3 m). Figure 7-6 also includes the instances of cavity fire spread depicted in Fig. 7-5, marked with dashed vertical lines. A dotted horizontal line at 800 K (1000°F) indicates the approximate point when flames reach the respective thermocouple locations. At about 1 min 30 s, the first sound of superstrate glass cracking is heard. At approximately 3 min 30 s, the CTC at the 4 ft location records a temperature of 800 K, coinciding with the shattering of substrate glass and CTC impingement from the 4 ft (1.2 m) tall propane fire source, as shown in Fig. 7-5(b). Following this, an accelerated fire spread is observed, with the CTC at the 14 ft (4.3 m) location reaching the 800 K threshold within approximately 45 seconds, corresponding to Fig. 7-5 (f). Between the flame travel from the 10 ft (3.0 m) to the 14 ft (4.3 m) CTC locations, the flame spread rate is approximately 25 cm/s (0.8 ft/s). It is important to note that the CTCs at higher locations, particularly at 14 ft (4.3 m) and 16 ft (4.9 m), do not record high flame temperatures due to metal flashing located at 16 ft height, entrapping smoke and displacing oxygen for cavity flames. Therefore, the CTCs at approximately 10 ft (3.0 m) or 12 ft (3.7 m) provided a better interpretation of cavity flame spread rate. For decisive measurements, point sources such as CTCs can be replaced by other techniques such as an array of CTCs or linear heat detectors (LHDs) such as [68].

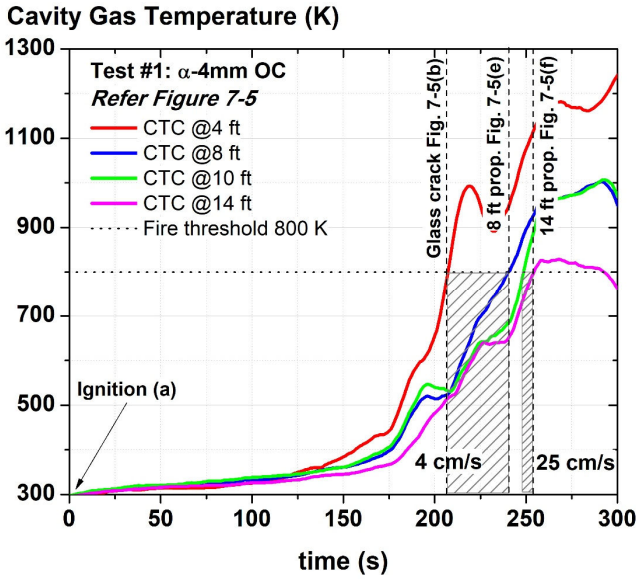

Figure 7-6: CTC profiles for Test #1 (α–4mm OC) at multiple heights — the instances (b), (e), and (f) correspond to photograph shown in Fig. 7-5.

In addition to monitoring cavity fire spread, it is essential to quantify the eventual flashover of cavity fires to exterior fires and the fuel contribution from falling PV panels onto the propane ignition source using other instrumentation. For this purpose, global measurement tools such as HRR and mass loss can provide a more comprehensive information on the dynamics of fire spread. Specifically, peak HRR data has shown a strong correlation with the vertical flame spread rate and the extent of propagation in 16-ft PPTs [15, 16]. Figure 7-7 presents two such global measurements for Test #1; this figure compares the HRR profile with that of the CTC at a 12 ft (3.7 m) height and also it with the mass loss data.

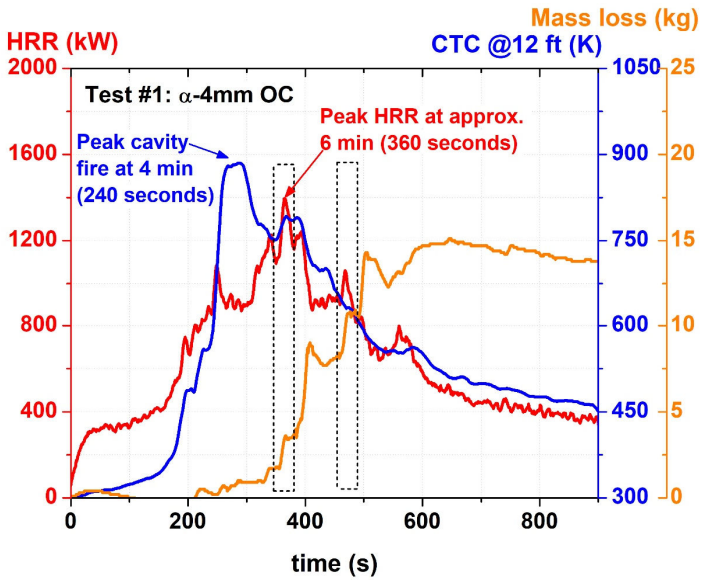

Figure 7-7: α–4mm OC 16-ft PPT (Test #1) HRR comparison with CTC at 12 ft, and mass loss profiles.

As previously mentioned, the CTC at 12 ft (3.7 m) provides representative information on cavity flame spread. Figure 7-7 shows that the HRR profile proportionally tracks the cavity temperature increase rate until approximately 300 s after ignition. After this point, the CTC decreases due to flashovers to an exterior fire and the falling of module debris, which opens the cavity and cools it with entraining air. The peak HRR occurs approximately one minute after the peak cavity temperature. Figure 7-7 also shows sudden, simultaneous spikes in mass loss and HRR data at the 360 s mark. These spikes are attributed to effect of the falling of module debris and its shattering on the propane burner, which instantly burns the plastic encapsulants sandwiched within glass superstrates and substrates. Some mass loss spikes are not accompanied by an increase in HRR. These spikes are due to metal joint/attachment systems falling from the BIPV façade setup outside the load cell area.

Unlike the fire propagation in traditional wall systems, such as sandwich panels [14, 69] and cladding wall panels [15, 16], BIPV system tests reveal a different phenomenon where the peak HRR is correlated not only with flame propagation distance but also with the falling of combustible module debris. A non-hazardous BIPV system should result not only in shorter flame spread distance but also lead to lower debris hazard. The peak HRR thresholds from the 16-ft PPT help in controlling both fire hazard factors. To further control debris hazard, failure criteria should include CTCs within the cavity to monitor cavity fire spread, the state of temperature-sensitive adhesives used to mount double-sided glass BIPV modules, and the structural integrity of the aluminum framing used to hold BIPV modules. Furthermore, criteria need to be added to assess the post-test condition of the uppermost BIPV modules. A cracked BIPV glass module can lead to pyrolysate gas emission and is also a debris hazard. Further discussion on these threshold criteria is provided in Section 7.1.3 and Section 8.

Figure 7-8 shows the post-test debris on the sand burner and load cell for Test #1. The debris mainly include large shards and molten pieces of glass, along with metal attachment joints. Additionally, bare copper cable wires with burned-out plastic jackets were visible, either hanging along the insulation or within the load cell/burner debris. Debris falling during fire tests is a major hazard related to BIPV facades. From a property insurance perspective, the combustible debris may cause secondary fires based on the configuration of the building and its façade.

An important observation from the post-test photographs is the presence of char on the MW insulation at the bottom edge of the 16 ft high panels. Figure 7-9 provides close-up photographs of the area near the bottom edge of the insulation after the test. This char originates from unburnt plastic from cable jackets, adhesives used in mounting systems, and plastic encapsulants, which flow downward toward the base of the setup.

(a) metal debris

(b) glass debris

Figure 7-8: Post-test debris photographs of Test #1.

(a) Test #3: γ–4mm OC

(b) Test #3: γ–4mm OC

(c) Test #2: β–3mm OC

Figure 7-9: Post-test photographs showing molten plastic on mineral wool at the setup base.

Among the three BIPV modules with 3-4 mm glass superstrates, the γ–4mm BIPV module has the thickest encapsulant, featuring 0.9 mm of EVA on both the superstrate and substrate sides. In contrast, the β–3mm BIPV module has the thinnest encapsulant, with 0.2 mm of POE on the superstrate side and none on the substrate side. Given that the densities of POE and EVA are similar [50], their relative difference in the thickness correlates with the peak HRR shown in Fig. 7-1. The peak HRR for the γ–4mm module (Test #3) is the highest, at 1600 kW, while the β–3mm module has a lower peak HRR of 1150 kW. The α–4mm module (Test #1) has a peak HRR of 1400 kW, which falls in the middle of these three BIPVs. These observations suggest that encapsulant thickness, as noted in Table 4-1, affects the combustible fuel loading and fire performance of BIPVs.

The γ–6mm BIPV module used in Test #4 also has a high encapsulant thickness, with 0.9 mm of EVA on both sides, but is protected by a 50% thicker glass (6 mm) compared to the γ–4mm modules. The combination of increased glass thickness and the use of cavity restrictors every 2 ft (0.6 m) results in the lowest peak HRR of 780 kW for the γ–6mm module (Test #4) among all modules tested in their uncharged states. The BIPV cavity wall fire dynamics are complex phenomena which require a large-scale façade test like 16-ft PPT for their evaluation. Based on the observations, several factors affect the fire performance of double-sided glass BIPV modules, including glass thickness, cavity design, and encapsulant thickness.

Figures 7-10 and 7-11 present plots for the β–3mm OC (Test #2) and γ–4mm OC (Test #3) 16-ft PPTs, respectively. These figures include CTC measurements at various heights, comparisons of HRR with CTC at 12 ft (3.7 m), and the mass loss profiles.

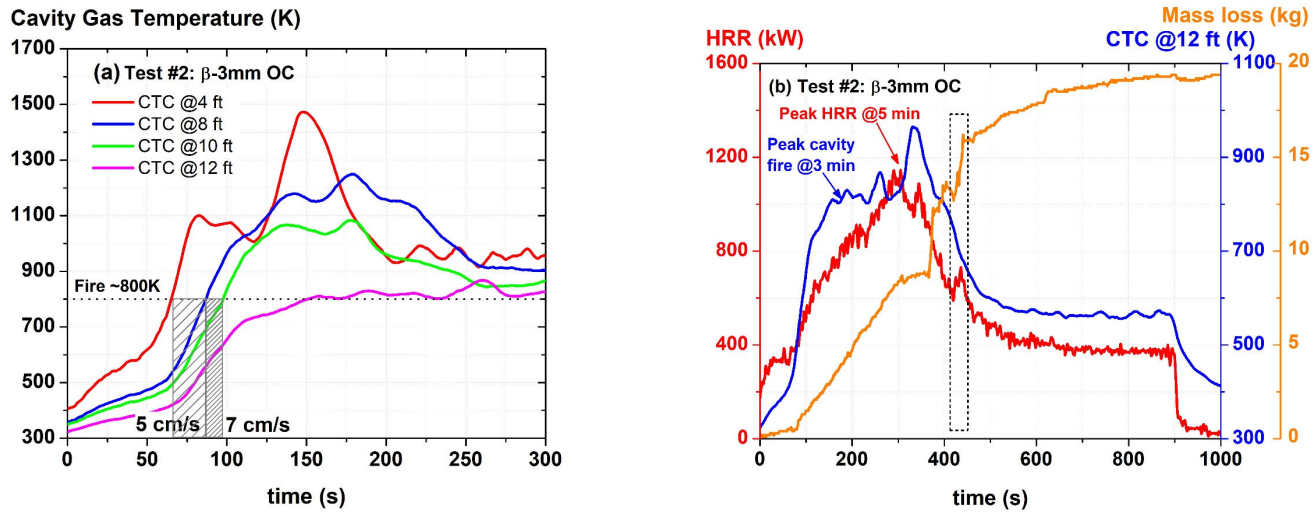

Figure 7-10: Plots for the β–3mm OC 16-ft PPT (Test #2): (a) CTC profiles at multiple heights, (b) HRR comparison with CTC at 12 ft, and with mass loss profiles.

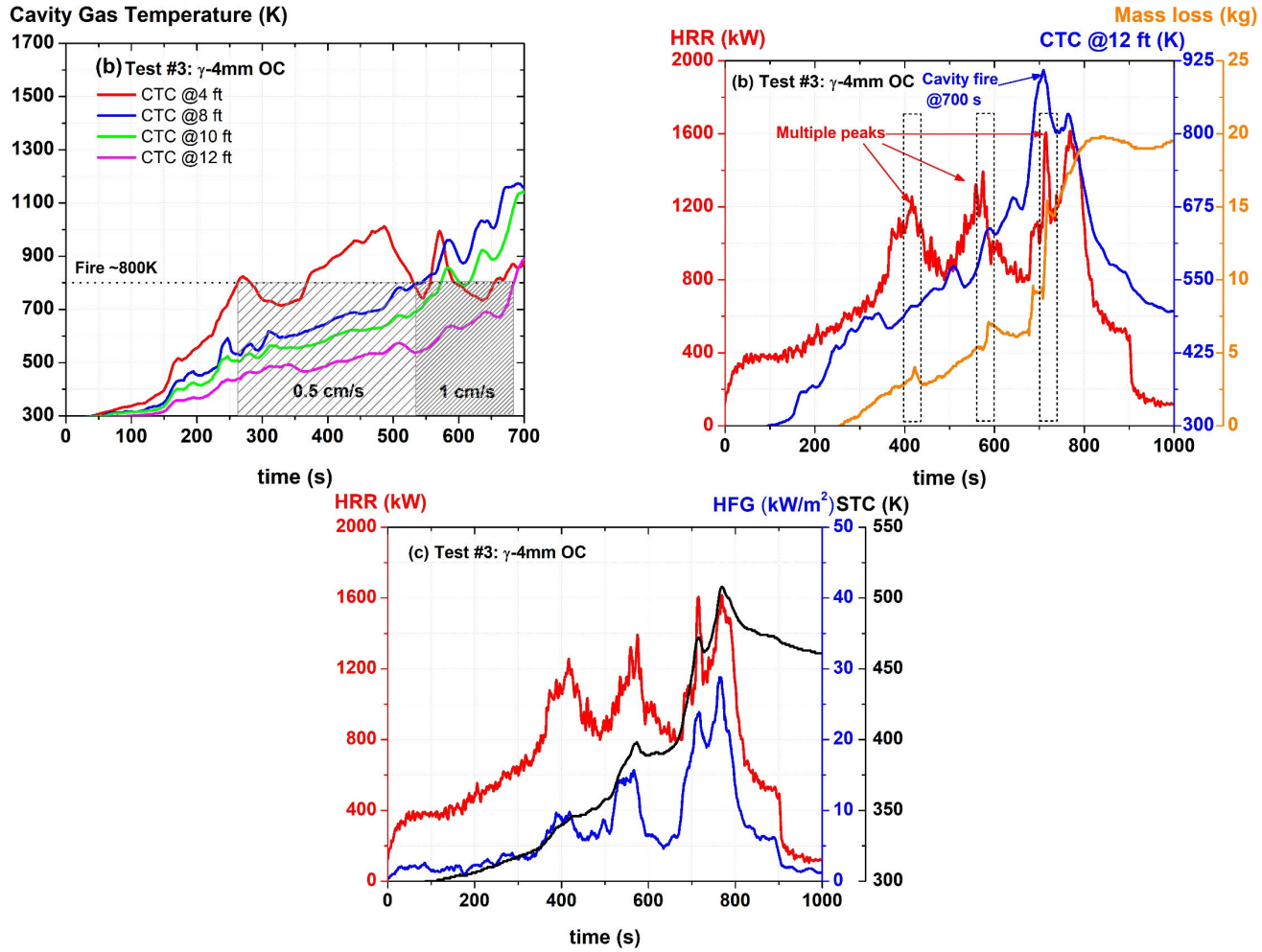

Figure 7-11: Plots for the γ–4mm OC 16-ft PPT (Test #3): (a) CTC profiles at multiple heights, (b) HRR comparison with CTC at 12 ft, and with mass loss profiles, and (c) HRR, HFG at 16 ft (4.9 m) and STC at 15 ft (4.6 m) profiles.

The results of Test #2 and Test #3 exhibit similarities to those of Test #1, which were presented above. However, there are some notable differences which are discussed next. In Test #2 with β–3mm OC, fire propagation within the cavity starts earlier due to the thinner glass (3 mm) used in these panels compared to the 4 mm thick glass of the α–4mm panels in Test #1. The thinner glass shatters sooner, approximately 60 s (compared to 90 s for the α–4mm test) after ignition, leading to earlier fire spread within the cavity. The HRR growth in Test #2 is primarily associated with cavity fire and exterior fire growth rather than contributions from falling panel debris. This is because the β–3mm panels have a thinner encapsulant layer (0.2 mm under the superstrate) compared to the α–4mm panels in Test #1 (0.6 mm under both superstrate and substrate). This results in less combustible material contributing to the fire when the β–3mm panels disintegrate from falling. For example, the marked mass loss spike in Fig. 7-10(b), from falling module debris, corresponds to only a 70 kW HRR spike. In comparison, the HRR spikes in α–4mm tests ranged approximately from 150 kW to 200 kW. Consequently, the combination of thinner glass and a thinner encapsulant layer in the β–3mm panels leads to earlier fire propagation within the cavity but a lower HRR contribution from falling debris, distinct from the dynamics observed with the thicker α–4mm panels in Test #1.

For the γ–4mm OC test (Test #3, see Fig. 7-11), the cavity fire spread, HRR, cavity fire growth, and mass loss develop more slowly than those observed in Tests #1 and #2. This variation is primarily attributed to the attachment system used in the γ–4mm panels, as previously shown in Fig. 6-2(b). The attachment system includes a horizontal joint located approximately every 2 ft (0.6 m), which effectively reduces the air cavity depth from 4 in. (100 mm) to 1.6 in. (41 mm). This reduces the flame passage thickness through the cavity and limits the flame heat flux within cavity, which in turn delays the shattering of substrate-side glass and release of fuel vapors within the cavity. The HRR spikes correlating to module shattering, shown in Fig. 7-11(b) are in the range of 100 to 500 kW. The upper range of 500 kW in γ–4mm (Test #3) is higher than that noted for α–4mm (150-200 kW) and β–3mm (about 70 kW) due to its higher encapsulant thickness and larger module size. A relatively larger γ–4mm module, containing higher mass of encapsulant fuel vapors, shatters and generates a higher HRR in comparison to α–4mm and β–3mm modules.

The impact of the horizontal joint systems can also be observed in Fig. 7-11(c), which shows the HFG data at 16 ft (4.9 m), STC on module at 15 ft (4.6 m), and HRR profiles for the γ–4mm OC 16-ft PPT (Test #3). The HFG and STC data exhibit peaks at the moments when a PV module falls or when the cavity fire flashovers to the exterior. Similar HFG and STC plots for Test #1 and Test #2 are presented in Appendix C.

Similar plots for the γ–6mm OC (Test #4) are shown in Fig. 7-12: it includes additional HFG data measured within the cavity of the setup at heights of 8 ft (2.4 m) and 12 ft (3.7 m) from the base. However, the mass loss data is missing due to an instrumentation error. The 6 mm thick superstrate and substrate glass modules significantly delay the shattering of the lowest PV module, and correspondingly, the entry of propane flames into the cavity. The CTC measurement at the 4 ft (1.2 m) location indicates fire penetration at approximately 390 s (6½ min) from ignition. In comparison, for the γ–4mm OC (Test #3), fire penetration within the cavity occurs at about 240 s (4 min) duration. The delay in the shattering of glass slows down the release of encapsulant fuel.

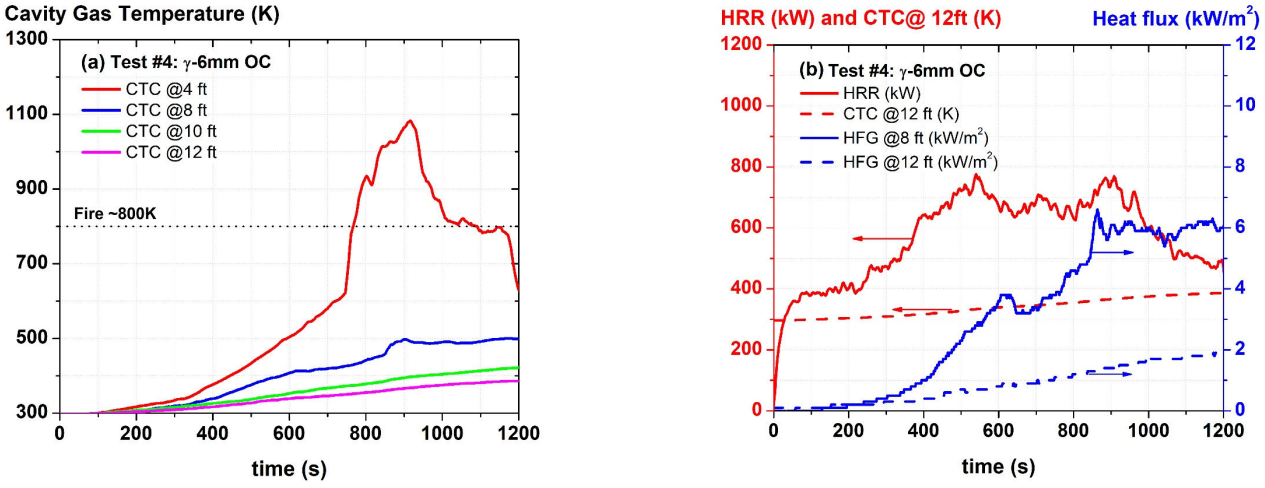

Figure 7-12: Plots for the γ–6mm OC 16-ft PPT (Test #4): (a) CTC profiles at multiple heights, (b) HRR comparison with CTC at 12 ft, and HFG located at 8 ft (2.4 m) and 12 ft (3.7 m) high cavity locations.

Furthermore, as previously shown in Fig. 6-2(c), the attachment system for the γ–6mm module uses cavity restrictors to compartmentalize the air cavity into 2 ft (0.6 m) high sections, thereby effectively eliminating air passages. These restrictors significantly reduce the flame spread rate within the cavity. The CTC recorded temperatures of less than 500 K at all heights of 8 ft (2.4 m) and above, as shown in Fig. 7-12(a).

Figure 7-12(b) compares the HRR, CTC at 12 ft (3.7 m) height, and the HFG data within the cavity at locations 8 ft (2.4 m) and 12 ft (3.7 m) above the burner. The peak HRR generated passes the ANSI/FM 4411 threshold for unlimited height installations, and the HFG data indicates the absence of flames at both the 8 ft (2.4 m) or 12 ft (3.7 m) high locations.

As mentioned in Table 4-1, the three BIPV modules used in Tests #1, 2, and 3 are accredited per EN 13501-1 or UL 1703; however, these accreditations do not correlate with their façade fire performance as evaluated by the 16-ft PPT method. An important conclusion from this discussion is the importance of evaluating the fire performance of the entire façade system, including its attachment details, and scenarios that accurately represent the hazards of façade fires. Assessing only the bench-scale flammability of the modules or subjecting them to non-representative fire scenarios, such as sloped-roof tests, may fail to adequately evaluate—and therefore improve upon—the true façade fire hazards of such systems.

7.1.2 Uncharged flexible BIPV

Figure 7-13(a) shows the peak propagation photograph of Test #5 with uncharged FlexPV. The fire propagated to the top of the setup within 1 minute of propane ignition, demonstrating a highly accelerating flame spread. The flames extended up to 10 ft (3.0 m) above the top of the 16 ft (4.9 m) high assembly before all the combustible material was consumed and the flames retreated to the ignition source. Figure 7-13(b) shows a post-test photograph confirming the consumption of almost all the BIPV material. The only debris left behind, as shown in Fig. 7-13(c), consisted of steel sheets used to provide bending flexibility to the FlexPV.

(a) peak propagation

(b) post-test panel

(c) post-test debris

Figure 7-13: Photographs from the FlexPV OC 16-ft PPT (Test #5)

Figure 7-14 shows the chemical HRR profile for Test #5. The peak HRR during the test was approximately 11 MW, and it quickly exceeded the ANSI/FM 4411 thresholds for all installation heights within 50 s from ignition.

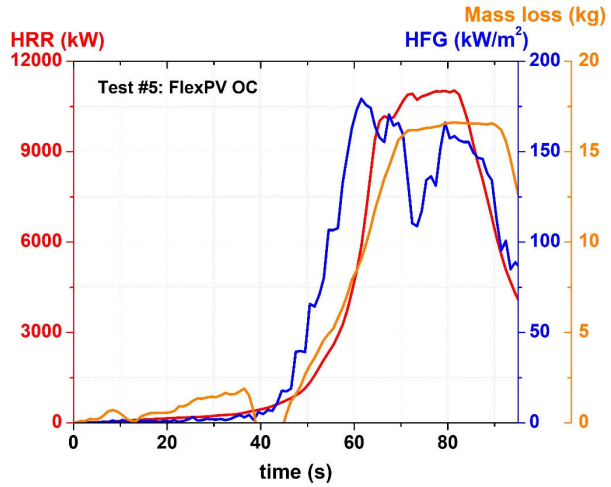

Figure 7-14: Results from the FlexPV OC 16-ft PPT Test #4: HRR profile, heat flux profile for a gage located at 16 ft (4.9 m) height above the base, and mass loss profile.

The total heat flux data for a gauge located at a 16 ft (4.9 m) height is shown in Fig. 7-14. During the test, the heat flux rapidly increased from nearly zero at 40 s from ignition to 180 kW/m^2 at 60 s from ignition. This rapid increase in heat flux indicates a highly accelerated surface flame spread in FlexPV. Unlike BIPV cavity-wall systems, the superstrate and substrate of FlexPV are made of laminated plastic (PET: Polyethylene terephthalate) with a thickness of 0.4 mm each. Since the encapsulant is only 0.2 mm thick on the superstrate end and none on the substrate end (as noted in Table 4-1), it is the laminated plastic that primarily contributes to the rapid vertical fire spread along the FlexPV surface. Furthermore, the lack of glass protection in FlexPV lead to a lower ignition resistance and thereby results in an accelerated fire propagation.

Lastly, Fig. 7-14 provides the mass loss profile for the FlexPV OC test. Unlike the BIPV cavity wall systems, where mass loss spikes occurred due to falling modules and attachment systems, no such spikes were observed for Test #5. The mass loss profile is relatively smooth, indicating it occurs primarily due to vertical surface flame spread. The total mass loss shown in Fig. 7-14 for the four FlexPV modules used in the 16-ft PPT is about 85% of their initial mass.

Despite being certified per UL 1703 as Class A material (Table 4-1), the FlexPV results highlight a significant issue. UL 1703 is a roof test that simulates a wind-driven fire, with the module separated a minimum of 36 in. (0.91 m) away from the roof leading edge. The test results underscore the importance of using an appropriate façade test that provides a realistic fire exposure to BIPVs in order to accurately assess their performance.

7.1.3 Module Charging Effects

This section discusses the 16-ft PPT fire spread results of charged BIPV wall systems, which include α–4mm MP (Test #6), γ–4mm MP (Test #7), γ–6mm MP (Test #8), and FlexPV MP (Test #9). Table 7-1 provides a comprehensive result data set for all 16-ft PPT results of this research. The results in Table 7-1 include the peak HRR generated during the test, the peak CTC measurements at 12 ft (3.7 m) height, the peak STC measurements at 15 ft (4.6 m) height on the BIPV superstrate, and the peak HFG at 16 ft (4.9 m) height. For γ–6mm tests (Tests #4 and #8), the peak in-cavity HFG data at 8 ft (2.4 m) and 12 ft (3.7 m) height are reported. The total mass loss data recorded during the test using the load cell is provided. The HRR and mass loss data are used to calculate the chemical heat of combustion (ΔH_C). Lastly, the peak cavity and exterior burnt height data from post-test analysis is compiled. The data in Table 7-1 will be referred to in this section for further discussions.

First, the effect of module charging on double-sided glass BIPVs is discussed. Figure 7-15 shows the HRR profiles for both uncharged and charged BIPV cavity wall systems. Figure 7-15(a) presents the results for α–4mm , comparing the uncharged test with the charged test. Similarly, Fig. 7-15(b) compares the HRR profiles of γ–4mm, and Fig. 7-15(c) compares that for γ–6mm tests in OC and MP states.

Table 7-1: Compilation of the 16-ft PPT results, including uncharged and charged tests.

Test #	BIPV and Configuration [Δ,X]	Peak HRR (kW)[^]	Total Mass Loss (kg)	ΔH_c (kJ/g)[#]	Peak CTC @12 ft (K)	Peak STC @15 ft (K)	Peak HFG @16 ft (kW/m^2)	Peak Burnt Height (ft)	
								Cavity	Exterior
1	α–4mm OC	1400	23	10.7	850	300	10	16	14
2	β–3mm OC	1150	21	9.6	970	450	10	16	16
3	γ–4mm OC	1600	23	17.8	910	510	30	16	16
4	γ–6mm OC	780	--	--	390	370	Cavity HFG 8,12 ft ↓	< 8	< 8
5	FlexPV OC	11000	17	24.1	NA	--	180	NA	16
6	α–4mm MP	2300	27	14.1	1,000	500	20	16	16
7	γ–4mm MP	2450	28	17.9	930	460	20	16	16
8	γ–6mm MP	850	--	--	400	370	Cavity HFG 8,12 ft ↓	< 8	< 8
9	FlexPV MP	10900	17	26.7	NA	1200	180	NA	16

[Δ] OC → Uncharged (power supplies turned OFF) and MP → Charged (power supplies are ON).
[X] Cables for the OC tests were connected in the same manner to MP tests, but the power supplies were turned OFF.
[^] ANSI/FM 4411 thresholds: Unlimited height at peak HRR ≤ 830 kW and 50-ft limited height installation at 830 kW < peak HRR ≤ 1,100 kW.
[#] Calculated from HRR and mass loss measurements, after subtracting the propane contribution.
CTC → cavity thermocouple | STC → surface thermocouple | HFG → heat flux gage | NA → Not applicable | -- instrumentation failure.
Cavity HFG Test #4 γ–6mm OC: @ 8 ft: peak HFG = 7 kW/m^2 | @ 12 ft: peak HFG = 2 kW/m^2.
Cavity HFG Test #8 γ–6mm MP: @ 8 ft: peak HFG = 7 kW/m^2 | @ 12 ft: peak HFG = 2 kW/m^2.

First, the results for α–4mm and γ–4mm modules, shown in Figs. 7-15(a) and (b), respectively, and Table 7-1 are discussed. The peak HRR of the MP charged α–4mm and γ–4mm modules is significantly higher than that of the uncharged modules. In the case of α–4mm , there is a 60% increase in the peak HRR, from 1400 kW for the uncharged system to 2300 kW for the MP charged system. Similarly, a 50% increase in peak HRR is noted for the γ–4mm OC test (1600 kW) compared to the γ–4mm MP test (2450 kW). Furthermore, the initial increase in HRR, which correlates with the breaking of glass and the rate of vertical cavity fire spread, occurs earlier for the MP cases of α–4mm and γ–4mm. For both modules, the cavity fire spread in the MP case occurs approximately 30 to 40 seconds earlier than in the OC case.

As discussed in Section 5, charging BIPV modules increases the temperatures of various components, including the superstrate/substrate glass, encapsulant, cables, and the insulation behind them. For encapsulants, the temperature may rise to a point where it changes its phase from a crystalline to a molten state. Specifically, the initial glass temperature rise for α–4mm MP is 38°F (21°C), while for γ–4mm MP it is 61°F (34°C), compared to the initial temperatures of the uncharged tests of the respective modules. A likely explanation for these observed behaviors is that, in these two MP-charged BIPVs, the expansion of the encapsulant, along with the increased thermal stress on the glass due to its elevated temperatures, contributes to the earlier shattering of the glass from propane flames. This earlier shattering allows propane flames to enter the cavity behind the bottom-most modules more quickly, resulting in an earlier cavity fire spread.

However, the results for the γ–6mm modules reveal that charging marginally increases the peak HRR from 780 to 850 kW. Furthermore, the HRR profiles are almost repeatable for the γ–6mm OC and MP tests, as shown in Fig. 7-15(c), and there is no evidence of quicker propagation in the MP test. There are a few possible reasons for the lack of change in the HRR profiles between the OC and MP tests of the γ–6mm modules: First, the thicker 6 mm glass superstrate and substrate modules have a higher heat capacity, resulting in an initial temperature increase of just 11°F (6°C) for MP modules compared to OC modules. The relatively similar temperatures for the OC and MP tests lead to similar glass shattering and resultant cavity flame spread dynamics. Secondly, the γ–6mm modules use a significantly higher amount of metal in their attachment/mounting system (cleats and stiffeners). These systems also increase the specific heat of the setup, leading to a lower temperature rise in MP charged state compared to the γ–4mm modules. Lastly, the shattering time for thicker tempered glass is higher [70], and hence the effects of glass shattering dynamics is less noticeable in thicker BIPV modules.

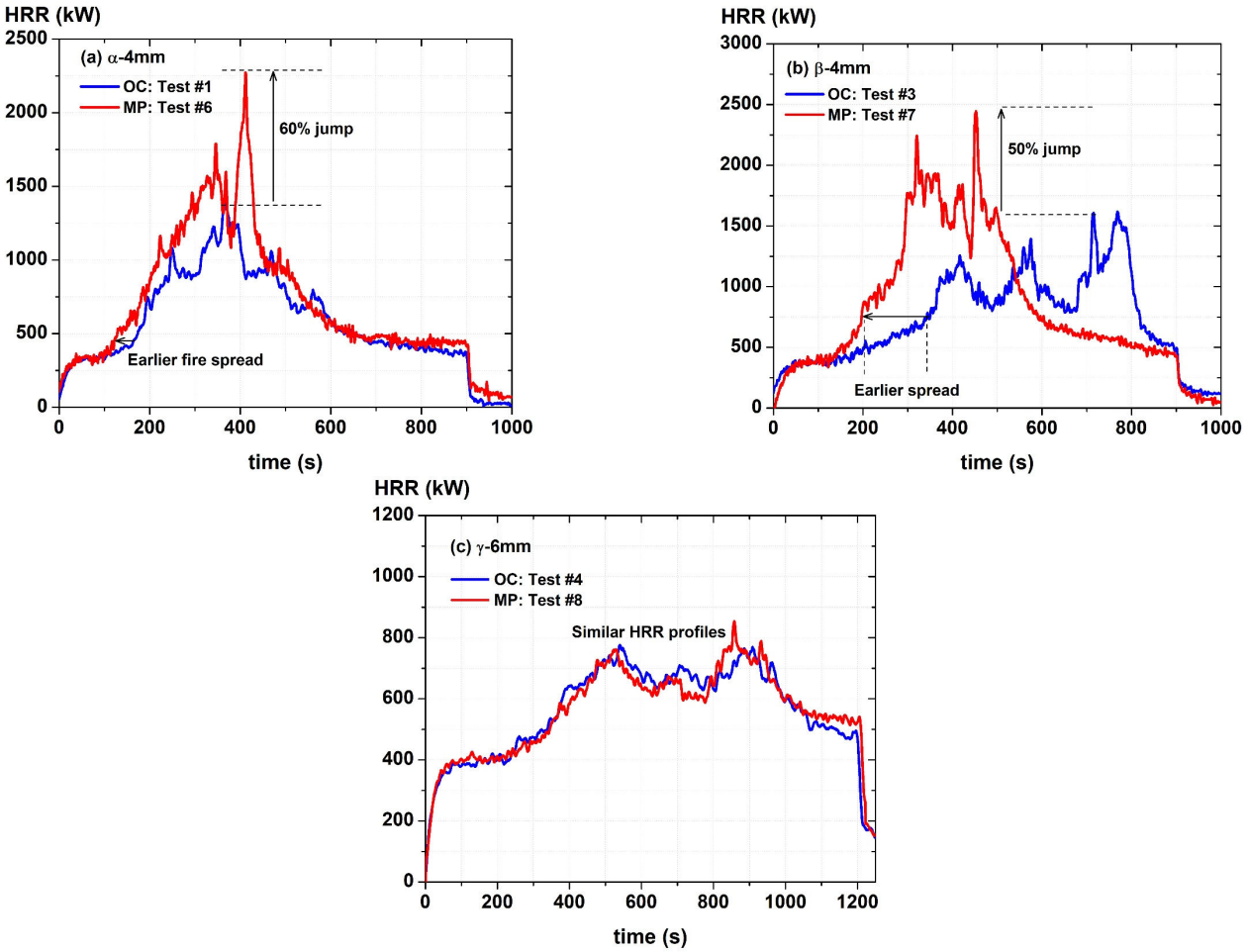

Figure 7-15: HRR comparison of uncharged and charged cavity-wall 16-ft PPTs (a) α–4mm OC (Test #1) vs. α–4mm MP (Test #6); (b) γ–4mm OC (Test #3) vs. γ–4mm MP (Test #7); and (c) γ–6mm OC (Test #4) vs. γ–6mm MP (Test #8).

Figure 7-16 shows the CTC data at 8 ft (2.4 m) and 12 ft (3.7 m) heights for the OC and MP tests of α–4mm , γ–4mm, and γ–6mm modules. Right at the ignition time (t = 0 s), the CTC records a higher temperature for the α–4mm and γ–4mm MP tests due to cavity air pre-heating. For the α–4mm MP case, glass cracking occurs approximately 2 minutes into ignition, compared to approximately 3 minutes and 20 seconds for the α–4mm OC case. Thereafter, the cavity fire spreads more quickly and earlier in the α–4mm MP test as compared to the α–4mm OC test.

In particular, for the γ–4mm OC test case, the horizontal joints at every 2 ft (0.6 m) vertical distance, that reduce the cavity depth from 4 in. (100 mm) to 1.6 in. (41 mm), acted as barriers to the spread of internal flames. This resulted in a relatively slower cavity flame spread. However, the γ–4mm MP case shows that, despite the presence of these cavity barriers, the fire propagation occurred earlier and noticeably faster than in the γ–4mm OC test case.

The glass shattering time range for the γ–6mm OC and MP cases is similar. Furthermore, except for the CTC at 8 ft (2.4 m), all other CTCs for the γ–6mm OC and MP tests showed similar profiles. Specifically, the CTC at 12 ft (3.7 m) reached a peak temperature of about 400 K for both OC and MP tests, indicating a limited cavity flame spread. The combination of thicker glass and restrictors that compartmentalize the cavity every 2 ft (0.6 m) significantly delays both the shattering of the glass by the propane flames and the cavity flame spread. The discrepancy of CTC at 8 ft (2.4 m) highlights the need of an array of CTCs or a linear heat detector to improve the reproducibility of 16-ft PPT measurements.

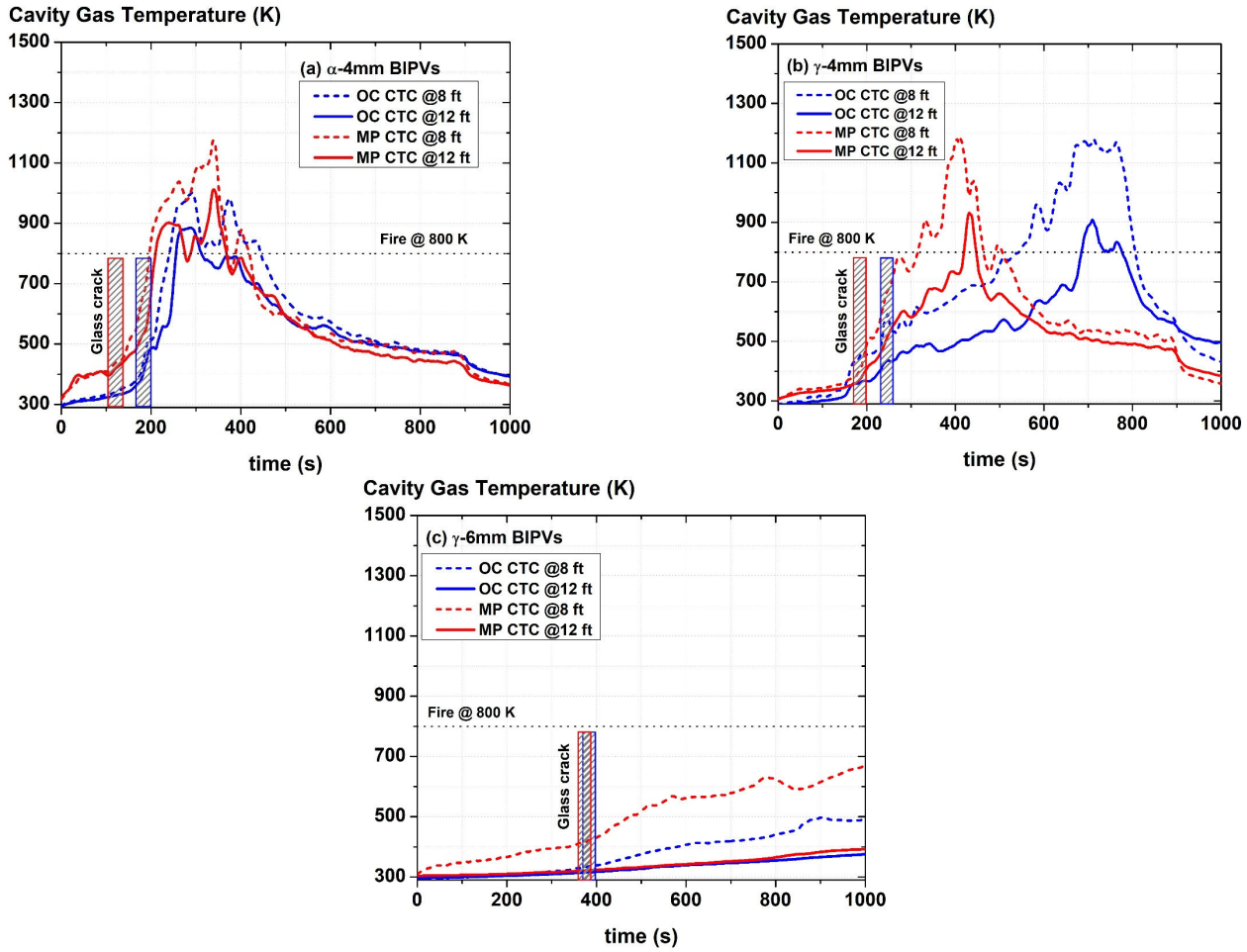

Figure 7-16: CTC measurement comparison of uncharged and charged cavity-wall 16-ft PPTs (a) α–4mm OC (Test #1) vs. α–4mm MP (Test #6); (b) γ–4mm OC (Test #3) vs. γ–4mm MP (Test #7); and (c) γ–6mm OC (Test #4) vs. γ–6mm MP (Test #8).

The mass loss comparison for the OC and MP test cases for α–4mm and γ–4mm BIPV systems is shown in Fig. 7-17. The profiles clearly demonstrate an earlier fire spread in the MP charged systems, with mass loss spikes indicating that the module and attachment falls occur earlier in the MP systems. Similar conclusions can be drawn from the STC and HFG profiles, which are presented in Appendix C. This data reinforces the observed trend that charged BIPV systems (MP tests) with up to 4 mm thick superstrate glass experience more rapid and aggressive fire spread and mass loss compared to their uncharged counterparts (OC tests).

Photographs at peak propagation for the α–4mm MP, γ–4mm MP, and γ–6mm MP cases are shown in Fig. 7-18, while the post-test damage photographs are depicted in Fig. 7-19. Consistent with the data presented in Table 7-1, these photographs confirm that the MP tests result in higher flame heights and greater post-test façade damage for both the α–4mm and γ–4mm BIPV systems. On the other hand, the peak propagation and the post-test damage of γ–6mm MP modules is similar to that of OC modules (shown in Figs. 7-2 and 7-3).

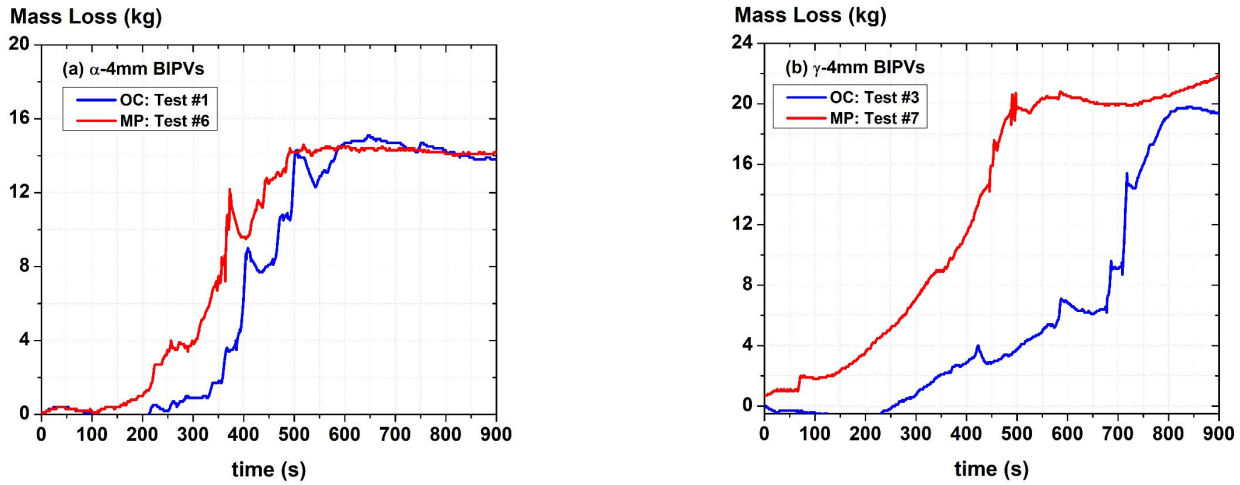

Figure 7-17: Mass loss comparison of uncharged and charged cavity-wall 16-ft PPTs (a) α–4mm OC (Test #1) vs. α–4mm MP (Test #6) and (b) γ–4mm OC (Test #3) vs. γ–4mm MP (Test #7).

(a) (b) (c)

Figure 7-18: Peak fire propagation instants of (a) α–4mm MP (Test #6), (b) γ–4mm MP (Test #7), and (c) γ–6mm MP (Test #8) tests.

Figure 7-20 illustrates the peak HRR instants and the post-test damage for the FlexPV MP (Test #9) test. Additionally, Fig. 7-21 presents comparative plots of HRR, mass loss, and HFG data for the FlexPV OC and FlexPV MP tests. The data from Fig. 7-21 and Table 7-1 indicate that the fire performance of the OC and MP panels for the FlexPV tests is similar. The HRR profiles, including the peak HRR and the spread rate of flame, are consistent between the two tests. Additionally, the total mass loss, which is 85% of the initial mass, and the peak heat flux value of 180 kW/m^2, are all the same for both OC and MP tests.

The similarities in fire performance between the OC and MP modules in the FlexPV tests stem from the absence of tempered glass superstrate and air cavity. The flame spread in the FlexPV tests is driven by the surface burning of the PET superstrate rather than cavity fire, as was observed in double-sided glass BIPVs. The melting point of PET is 500°F (260°C), which is much higher than the operating temperature of FlexPV under MP conditions (122°F, 50 °C, as noted in Appendix A) and the encapsulant melting temperature (104-140°C, 40-60°C, as discussed in Section 5.2). Therefore, when operating under MP conditions, the flammability of the PET superstrate, and hence that of FlexPV modules, remains similar to that in the OC condition test at ambient temperature. Therefore, the absence of glass and air cavity, combined with the surface burning dynamics governed by the PET superstrate, are key reasons why the FlexPV exhibits similar fire performance under both OC and MP conditions.

(a) (b) (c)

Figure 7-19: Post-test photographs of (a) α–4mm MP (Test #6), (b) γ–4mm MP (Test #7), and (c) γ–6mm MP (Test #8) tests.

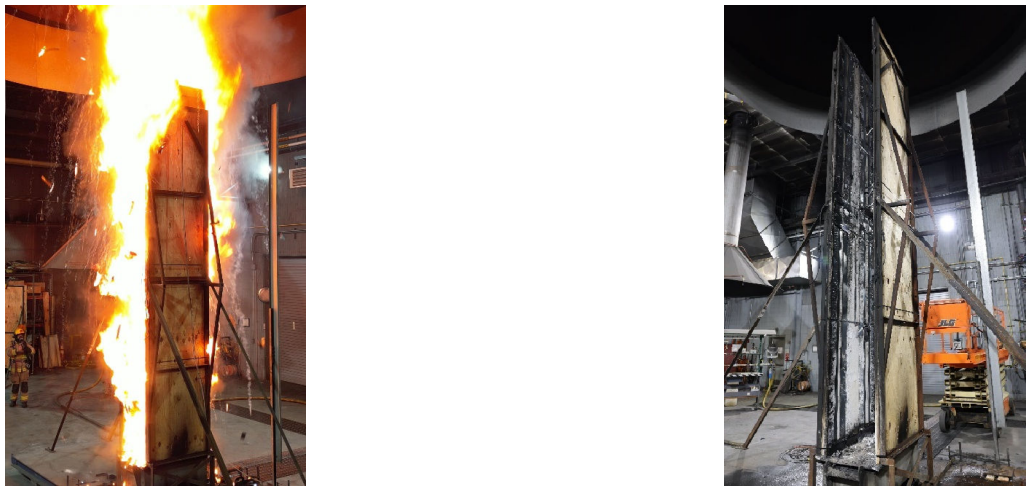

(a) (b)

Figure 7-20: FlexPV MP (Test #9) photographs: (a) peak HRR instant, and (b) post-test damage.

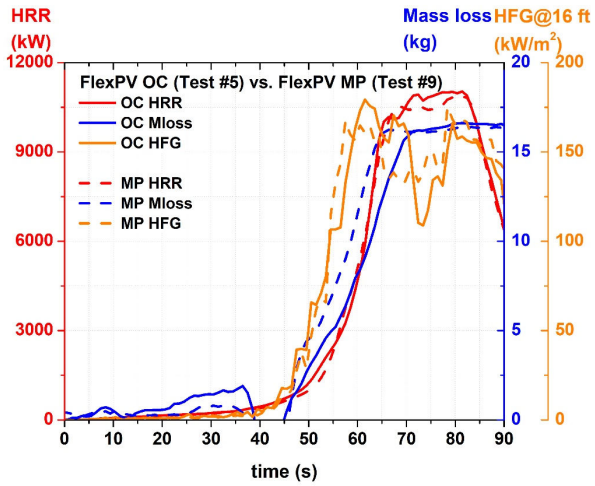

Figure 7-21: Comparison of FlexPV OC (Test #5) and MP (Test #9) data: HRR, mass loss, and HFG at 16 ft (4.9 m) height.

In conclusion, charging a BIPV module may increase hazards depending on factors such as glass thickness, cavity restrictors, and whether the module is a double-sided glass or flexible PV. However, uncharged state 16-ft PPTs provided sufficient data to evaluate cavity and external flame spread from the HRR and CTC measurements: systems that either propagated or did not propagate in OC tests exhibited similar behavior during MP tests. Additionally, charging BIPV modules by forcing reverse current may not be feasible, particularly if the junction box prevents it, as observed with β–3mm modules. Therefore, it is recommended to conduct BIPV 16-ft PPTs in uncharged (or OC) states.

The pass-fail criteria for BIPV 16-ft PPTs will differ from those of ANSI/FM 4411. While the latter relies solely on peak HRR thresholds to determine the acceptability of wall systems, the BIPV 16-ft PPTs have highlighted certain issues with this approach.

Firstly, it is recommended that the peak HRR thresholds remain similar to those of ANSI/FM 4411: unlimited height installation for peak HRR ≤ 830 kW and a 50-ft limited height installation for 830 kW < peak HRR ≤ 1100 kW. HRR spikes in the range of 150-200 kW may occur during tests due to the shattering of double-sided glass BIPV modules onto the propane burner — events unrelated to the vertical flame spread physics used to develop HRR thresholds —thus providing an argument for making these HRR thresholds less conservative. However, since fire tests are conducted with modules in an uncharged state, potentially resulting in lower peak HRR compared to realistic conditions when modules are heated by solar radiation and Joule heating, maintaining the current HRR thresholds is justified.

Secondly, cavity fire spread is the primary dynamic of fire growth within double-sided glass BIPV systems, so it is recommended to include a criterion for monitoring the cavity flame spread. Additionally, high temperatures within the cavity can lead to the burning or degradation of module mounting adhesives and affects the structural integrity of aluminum mount systems [71] — both factors lead to the falling debris hazard, and further underscore the need of monitoring cavity temperatures.

Lastly, due to the nature of double-sided glass BIPV systems, even if the fire propagates externally, the final evaluation must assess whether flames and thermal stress can damage the non-combustible glass façade. A cracked or shattered glass is a source of pyrolysate gases and debris hazard. Therefore, revised 16-ft PPT criteria for BIPVs are needed that account for HRR, cavity temperature monitoring, and the damage state of modules at the end of the test. The recommended 16-ft PPT pass-fail criteria are discussed in Section 8.

7.2 8-ft CWT

Table 7-2 details the test results for the three 8-ft CWTs. These results include the peak HRR, peak flame spread distance, peak CTC (at 6 ft or 1.8 m height), peak BIPV STC (at 6 ft or 1.8 m height), and the peak HFG data (at 6 ft or 1.8 m height). The profile plots for HRR, CTC, STC, and HFG are shown in Fig. 7-22.

Table 7-2: Compilation of the 8-ft CWT results.

Test #	BIPV and configuration [Δ,X]	Peak HRR (kW)[^]	Peak CTC @6 ft (K)	Peak STC @6 ft (K)	Peak HFG @6 ft (kW/m²)	Peak flame height (ft)
10	α–4mm MP	22	430	340	4	< 4
11	β–3mm OC	17	410	330	3	< 4
12	γ–4mm MP*	14	440	370	4	< 4

[Δ] OC → Uncharged (power supplies turned OFF) and MP → Charged (power supplies are ON).
[X] Cables for the OC tests were connected in the same manner to MP tests, but the power supplies were turned OFF.
[^] FM 4411 thresholds: peak HRR ≤ 100 kW flame height < 6 ft (1.8 m).
* CTC, STC, and HFG instrumentation at 5 ft height.
CTC → cavity thermocouple | STC → surface thermocouple | HFG → heat flux gage.

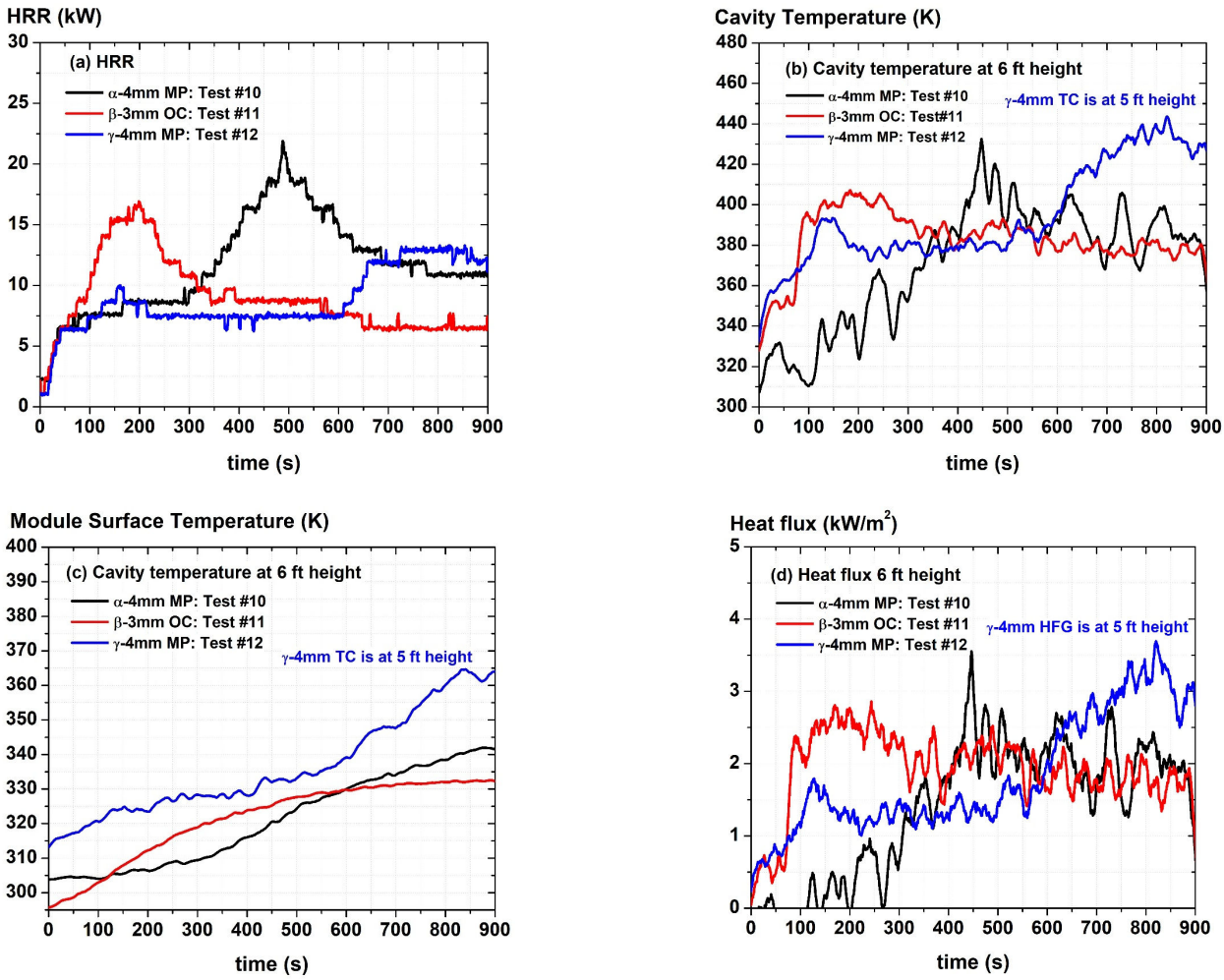

Figure 7-22: Measurements from the 8-ft CWTs (Tests #10-12): (a) HRR, (b) CTC at 6 ft height, (c) Module STC at 6 ft height, and (d) HFG in cavity at 6 ft height.

The ANSI/FM 4411 protocol uses a peak HRR threshold of 100 kW and a flame height threshold of 6 ft (1.8 m) for its pass/fail criteria. All three tests passed the peak HRR and flame height thresholds. Figure 7-23 shows the peak flame spread instant for the three tests: the flame heights are lower than 4 ft (1.2 m) for all three tests.

The post-test damage photographs of Tests #10 to #12 are shown in Fig. 7-24. All three tests indicate localized damage around the propane flame impingement zone, along with approximately 4 ft (1.2 m) of burnt cable lengths. In the α–4mm (Test #10) and γ–4mm (Test #12) CWTs, the propane flames in the cavity could not penetrate the 4 mm thick substrate and superstrate glass. However, the 2 mm thick substrate and 3 mm thick superstrate glass of β–3mm (Test #11) were breached by the propane flames in the cavity. Compared to the 16-ft PPT, the cavity fire spread was not significant since the propane flame preheating area (~ 1.5 ft or 0.5 m [49]) is limited in the 8-ft CWT. This limitation results in a lower planar direction thermal stress, along with the length and width of substrate glass from the cavity fire. In contrast, the preheating area in 16-ft PPTs is approximately 4 ft (1.2 m) high, which corresponds to the height of individual modules (5 ft or 1.5 m). Such fire exposure results in a high planar temperature gradient along the glass modules resulting from its thermal expansion and thereafter leads to an earlier glass shattering dynamics [67, 72]. These results demonstrate that the cavity fire spread hazard for double-sided glass BIPV facades is better captured in larger-scale 16-ft PPTs.

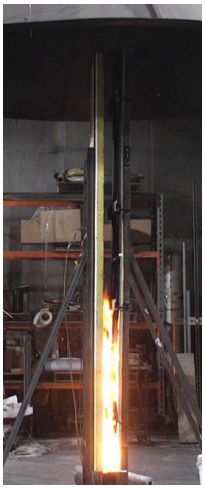

(a) α–4mm MP (Test #10)

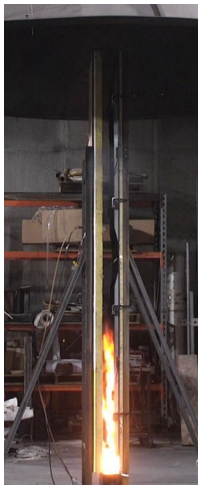

(b) β–3mm OC (Test #11)

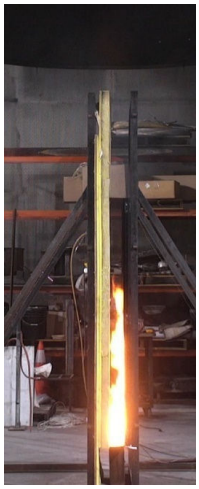

(c) γ–4mm MP (Test #12)

Figure 7-23: Peak propagation photographs of the 8-ft CWTs.

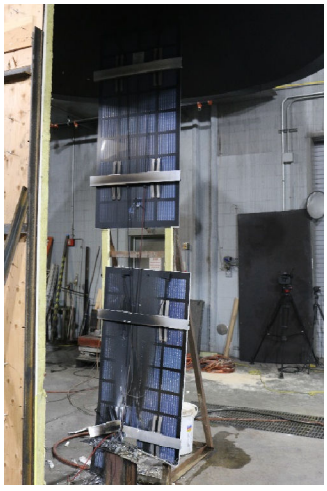

(a) α–4mm MP (Test #10)

(b) β–3mm OC (Test #11)

(c) γ–4mm MP (Test #12)

Figure 7-24: Post-test photographs of the 8-ft CWTs showing the module size exposed to cavity fire.

Lastly, an interesting observation was made during the post-test suppression of Test #10 with the α–4mm module. As described in Fig. 7-25, water was applied to the α–4mm module's superstrate glass near the propane impingement area during the post-test suppression routine. The hot module developed an approximately 6 in. (150 mm) tall crack along the centerline base of the setup due to thermal stress, causing hot pyrolysates from the gasified encapsulants to be ejected. The pyrolysates ignited instantly, producing a fireball that lasted about 0.5 seconds. This event shed light on how, during the 16-ft PPTs, the hot and gasified encapsulants trapped within the glass eventually contribute to cavity and external flame spread.

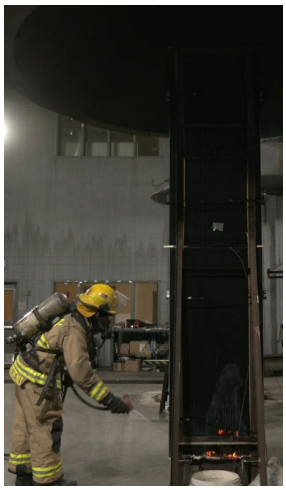

(a) before water application

(b) glass crack and pyrolysate ejection

(c) 0.1 s into pyrolysate ejection

(c) 0.5 s into pyrolysate ejection

Figure 7-25: Chronological events on water application on hot α–4mm BIPV module's superstrate glass.

8. Summary and Recommendations

The primary objectives of this research were to investigate the fire hazards of various BIPV façade systems using large-scale façade fire tests and provide recommendations to develop a new FM approval standard. For this purpose, four types of double-sided glass BIPV cavity wall systems, each differing in glass thickness, module size, solar cell technology, encapsulant type, and cavity details, were obtained, along with one flexible BIPV module type. Systems representative of field installations were constructed for 16-ft PPT and the 8-ft CWT large-scale façade testing. Non-combustible mineral wool insulation was used behind the air cavity, which was 4 to 4.75 in. (100 to 120 mm) depth, with interconnected electrical cables to simulate realistic installations.

Tests were conducted with BIPV modules in both uncharged and maximum power (MP) charged states. For the charged tests, an external power source provided reverse current to increase the temperature of the PV modules per the Joule heating effect, assessing the system's fire performance in field-like conditions.

The 16-ft PPT results for uncharged BIPV cavity-wall façade systems effectively captured the fire spread dynamics. During the tests, propane flames from the burner shattered the bottom BIPV glass modules, allowing flames to enter the cavity. Fire propagation within the cavity was driven by pyrolysates from cables and plastic encapsulants released after the shattering of substrate glass. As the fire spread up the cavity, flames spilled over the exterior through various joint openings, eventually causing the adhesives (used to mount modules) to burn and significant debris to fall onto the burner. The falling and shattering of BIPV modules onto the propane burner ignited the combustible plastic encapsulants, causing further HRR spikes. The results highlighted the need to evaluate the complete BIPV façade system using a relevant large-scale façade fire test such as 16-ft PPT.

The 16-ft PPT results of two MP-charged double-sided glass BIPV façades with 4 mm glass superstrates revealed higher fire hazards compared to their uncharged counterparts. Initial glass shattering and subsequent cavity fire propagation occurred more rapidly, and the peak HRR was 50 to 60% higher than in the uncharged façade tests. The increased fire hazard was attributed to the higher shattering propensity of preheated BIPV glass. However, BIPV systems with thicker 6 mm glass superstrates exhibited less of such a propensity, potentially attributable to marginal preheating due to their higher heat capacity, and hence the MP charged system demonstrated a similar fire performance to that of the uncharged system.

The results from the flexible BIPV tests revealed accelerated flame spread, with a maximum flame height much higher than the 16 ft (4.9 m) height of the setup. The peak HRR measured approximately 11 MW within 100 seconds of ignition for both OC and MP tests. Unlike the double-sided glass BIPV cavity-wall systems, the flexible BIPV's laminated plastic superstrate allowed surface flame spread to dominate the vertical fire growth.

The 8-ft CWT of double-sided glass BIPV systems showed no fire spread. The propane burner exposure and the preheated area were insufficient to shatter the tempered glass and release its plastic encapsulants, which were key factors driving the fire dynamics observed in the 16-ft PPTs.

Lastly, while BIPV modules are accredited by EN 13501-1 bench-scale and UL 1703 sloped-roof fire tests, these do not correlate with their actual façade fire performance as shown by the 16-ft PPT method. It's essential to assess the fire performance of the entire façade system, including attachment details, in realistic scenarios to accurately capture fire hazards. Simply evaluating bench-scale flammability or using non-representative tests may lead to inadequate assessments of BIPV façade fire risks.

Table 8-1 provides recommendations for developing a BIPV façade test standard. The recommendations include aspects pertaining to test setups, configurations, instrumentation, and pass-fail criteria. The reasonings behind these recommendations were discussed in Section 7, and are also compiled following Table 8-1.

Table 8-1: Testing, instrumentation, and pass/fail recommendations for BIPV façade standard.

<table>
<tr><th rowspan="2">BIPV type</th><th colspan="2">16-ft PPT[Δ] – Uncharged state tests</th><th colspan="2">8-ft CWT[Δ]– Uncharged state tests</th></tr>
<tr><th>Instrumentation</th><th>Pass/fail criteria</th><th>Instrumentation</th><th>Pass/fail criteria</th></tr>
<tr><td>Module:
Double-sided glass

Cavity:
present</td><td rowspan="2">• Standard 16-ft PPT.

• Array of 3 CTCs or 1 LHD each on both side panels at 12 ft (3.7 m) height.

o Temperature at 1 in. (25 mm) distance from insulation or backing.</td><td rowspan="2">Unlimited ht.:
Peak HRR ≤ 830 kW

50-ft (15 m) limited ht.:
830 kW < Peak HRR ≤ 1100 kW
+
CTC/LHD @12 ft < 473 K or 200 °C
+
No front glass cracking or shattering in top 4 ft (1.2 m) of modules</td><td colspan="2">• Not required if insulation is non-combustible.

• With combustible insulation, use guidance for glass faced/plastic backed modules.</td></tr>
<tr><td>Module:
Glass faced plastic backed

Cavity:
present</td><td>• Standard 8-ft CWT

• Array of 3 CTCs or 1 LHD at 6 ft (1.8 m) height</td><td>Peak HRR < 100 kW
+
No visual flames @ 6 ft
Or [Optional]
CTC/LHD @6 ft < 800 K or 525 °C</td></tr>
<tr><td>Module:
Flexible plastic – self adhered

Cavity:
absent</td><td>Standard 16-ft PPT</td><td>Follow ANSI/FM 4880/4881

Unlimited ht.:
Peak HRR ≤ 830 kW

50-ft (15 m) limited ht.:
830 kW < Peak HRR ≤ 1100 kW</td><td colspan="2">Not required</td></tr>
<tr><td colspan="5">[Δ] Cables for the tests should be interconnected, the same as field conditions.
CTC → cavity thermocouple | LHD → linear heat detector.</td></tr>
</table>

a. The 16-ft PPT effectively captures all relevant fire spread dynamics and is the recommended test for evaluating BIPV systems. The 8-ft CWT can be exempted for double-sided glass BIPV systems with non-combustible backing, but should be maintained for systems with plastic substrate modules or those with combustible insulation backing.

b. The test configuration should include the entire façade system, encompassing BIPV modules, cables, insulation, air cavity, and mounting system to assess flame spread hazards. Modules should ideally have centrally located vertical joints. Interconnected cabling should form a series of modules on each panel of the 16-ft PPT to capture their role in cavity fire dynamics.

c. Charging a BIPV module can increase fire spread hazards depending on factors like glass thickness, cavity restrictors, and the module type (double-sided glass or flexible). However, tests on non-propagating BIPV system show minimal differences, indicating charge status may not have a clear effect on non-propagating systems. Additionally, charging BIPV modules by reverse current might be infeasible if the junction box prevents it, as encountered with β–3mm modules. Consequently, it is advised to perform BIPV 16-ft PPTs in uncharged conditions.

d. The instrumentation should be enhanced to better evaluate cavity fire spread in the 16-ft PPTs. It is recommended to add either an LHD or an array of CTCs (minimum 3) installed at 12 ft ± 4 in. (3700 ± 100 mm) height. These should be placed on both wall panels of the 16-ft PPT and exposed 1 in. (25 mm) from the insulation layer surface, facing the substrate side of the BIPV modules. Similar instrumentation should be added to better capture the cavity fire spread in the 8-ft CWT.

e. The pass-fail criteria for BIPV 16-ft PPTs will differ from those in ANSI/FM 4411, which rely solely on peak HRR thresholds. Firstly, it is recommended that the peak HRR thresholds remain similar to those of ANSI/FM 4411, for the reasons discussed in Section 7.1.3. Next, cavity fire spread is the primary factor in fire growth within double-sided glass BIPV systems, requiring it to be monitored. Additionally, burning adhesives in the module mounting system and structural

integrity of aluminum mounts in high temperature environment creates debris hazard, emphasizing the need for cavity temperature monitoring. Lastly, if fire spreads externally, the evaluation must assess the thermal damage to the non-combustible glass façade, as cracked or shattered glass can be a source of pyrolysate gases and debris hazard.

Approval of BIPV cavity wall systems can be granted if all of the following three performance criteria for 16-ft PPTs are met.

i. Peak HRR ≤ 830 kW for unlimited height and 830 kW < peak HRR ≤ 1100 kW for 50-ft (15 m) height installation:
The peak HRR criterion remains similar to that in ANSI/FM 4411 or ANSO FM 4880/4881.

ii. Cavity temperature at 12 ft (3.7 m) height ≤ 473 K (200 °C):
The cavity temperature threshold of 473 K (200 °C) is recommended to limit cavity fire spread, to ensure that module mounting adhesives are protected, and the aluminum mounting systems retain their structural integrity. Cavity temperature should be tracked via LHD or an array of CTCs (minimum 3), placed on both wall panels of the 16-ft PPT. A 15 second moving average of individual thermocouples should be used for evaluation against the threshold.

iii. The top 4 ft (1.2 m) of PV modules remain undamaged:
The damage assessment criterion requires the superstrate glass of the top 4 ft (1.2 m) of PV modules to remain undamaged, meaning there should be no glass cracking or shattering. This ensures PV glass remains intact to prevent pyrolysates escape and excessive debris falling during a fire event. Module glass state can be monitored via cameras during the last 5 minutes of 16-ft PPTs, after the propane burner is turned off and before the application of water hose to cool the setup.

f. For flexible PVs that do not contain an air cavity, the ANSI/FM 4880/4881 thresholds should be used for 16-ft PPTs, *viz*. peak HRR ≤ 830 kW for unlimited height and 830 kW < peak HRR ≤ 1100 kW for 50-ft (15 m) height installation.

g. The evaluation criteria for the 8-ft CWT remain unchanged, *viz*. peak HRR ≤ 100 kW and maximum flame height is at 6 ft (1.8 m). Optionally, the current subjective measurement of maximum flame height can be replaced with a cavity temperature measurement at 6 ft (1.8 m), which should not exceed 800 K (525 °C).

Phase II of the BIPV research is underway and will further assess the effectiveness of various passive protection solutions for BIPV fire hazards, including cavity barriers, cable protection, and vertical separation distances.

Nomenclature and Abbreviations

Nomenclature

ΔH_C	Chemical heat of combustion (kJ/g)
I_{MP}	Maximum current flows out of the module when operating at the standard test conditions (1000 W/m^2 solar irradiation) (A)
I_{SC}	Maximum current flows out of the module when the module terminals are short-circuited (1000 W/m^2 solar irradiation) (A)
P_{MP}	Power PV module generates at the standard test conditions (1000 W/m^2 solar irradiation) (W); P_{MP} (= $V_{MP} \times I_{MP}$)
R	Resistance of PV module (Ω)
V_{MP}	Voltage PV module generates at the standard test conditions (1000 W/m^2 solar irradiation) (V)
V_{OC}	Maximum voltage PV module generates in an open circuit condition (V)

Abbreviations

ACM	Aluminum composite material
a-Si	Amorphous silicon
BAPV	Building-attached photovoltaic
BIPV	Building-integrated photovoltaic
CdTe	Cadmium telluride
CIGS	Copper-indium-gallium-diselenide
CIS	Copper-indium-selenide
CZTS	Copper-zinc-tin-sulfide
c-Si	crystalline silicon
CTC	Cavity thermocouple
ETFE	Ethylene Tetrafluoroethylene
EVA	ethylene vinyl acetate
GaAs	Gallium-Arsenide
HFG	Heat flux gage
HPL	High-pressure laminate

HRR	Heat release rate
IMP	Insulated metal sandwich panels
LHD	Linear heat detector
mc-Si	Multi-crystalline silicon
MP	Maximum power
MW	Mineral wool
µ-Si	Micromorphous silicon
OC	Open circuit
OPV	Organic photovoltaic
PE	Polyethylene
PET	Polyethylene terephthalate
POE	Polyolefin
PPE	Polyphenylene ether
PVA	Polyvinyl acetate
SC	Short circuit
sc-Si	Single-crystal silicon
STC	Surface thermocouple
TPO	Thermoplastic polyolefin

References

1. K. Berger, A. B. Cueli, S. Boddaert, M. Del Buono, V. Delisle, F. Frontini, *et al.*, "Report IEA-PVPS T15-04: 2018: International definitions of “BIPV”," Report number IEA-PVPS T15-04: 2018, https://iea-pvps.org/wp-content/uploads/2020/02/IEA-PVPS_Task_15_Report_C0_International_definitions_of_BIPV_hrw_180823.pdf

2. B. Meacham and M. McNamee, "Fire safety challenges of ‘green’buildings and attributes," The Fire Protection Research Foundation, Final Report, Report Number FPRF-2020-13, 1 October 2020. https://www.nfpa.org/education-and-research/research/fire-protection-research-foundation/projects-and-reports/fire-safety-challenges-of-green-buildings

3. *London Fire: A Visual Guide to What Happened at Grenfell Tower*, 2017.(Accessed on: November 20, 2017) Available: http://www.bbc.com/news/uk-40301289

4. *At least five killed as blaze engulfs apartment blocks in Spain's Valencia*, 2024.(Accessed on: 23 February, 2024) Available: https://www.bbc.com/news/world-europe-68374811

5. J. Anderson, L. Boström, R. Chiva, E. Guillaume, S. Colwell, A. Hofmann, and P. Tóth, "European approach to assess the fire performance of façades," *Fire and Materials,* vol. 45 (5), pp. 598-608, 2021. https://doi.org/10.1002/fam.2878

6. M. Moore-Bick, "Grenfell Tower Inquiry: Phase 1 Report," ISBN 978-1-5286-1602-7, October 2019. https://www.grenfelltowerinquiry.org.uk/

7. M. Moore-Bick, A.-A. Obe, and T. Istephan, "Grenfell Tower Inquiry: Phase 2 Report," ISBN 978-1-5286-5080-9, September 2024. https://www.grenfelltowerinquiry.org.uk/

8. M. Bergius, "Comparison of Two Test Methodologies for Fire Testing of Façade Systems," RISE Research Institutes of Sweden, Report number 2023:29, Project number 130011-05B, 2023. https://risefr.com/media/rapporter/comparison-of-two-test-methodologies-for-fire-testing-of-facade-systems-3.pdf

9. *Inquiry Phase 2 Response – The Future of Fire Testing*, 2024.(Accessed on) Available: https://www.thefpa.co.uk/news/inquiry-phase-2-response-the-future-of-fire-testing

10. *Review of the Ban on the use of Combustible Materials in and on the External Walls of Buildings*, 2020.(Accessed on) Available: https://www.gov.uk/government/consultations/review-of-the-ban-on-the-use-of-combustible-materials-in-and-on-the-external-walls-of-buildings

11. BS 9414, *Draft BS 9414 Fire performance of external cladding systems - The application of results from BS 8414-1 and BS 8414-2 tests*. London, UK: British Standards Institution (BSI), 2019.

12. NFPA-285, *Standard Fire Test Method for Evaluation of Fire Propagation Characteristics of Exterior Non-Load-Bearing Wall Assemblies Containing Combustible Components*. Quincy, MA, USA: National Fire Protection Association, 2025.

13. R. L. Alpert and R. J. Davis, "Evaluation of Exterior Insulation and Finish System Fire Hazard for Commercial Applications," *Journal of Fire Protection Engineering,* vol. 12 (4), pp. 245-258, 2002. http://dx.doi.org/10.1106/1042391031317

14. S. Nam and R. G. Bill, "A New Intermediate-scale Fire Test for Evaluating Building Material Flammability," *Journal of Fire Protection Engineering,* vol. 19 (3), pp. 157-176, 2009. http://dx.doi.org/10.1177/1042391508101994

15. G. Agarwal, "Evaluation of the Fire Performance of Aluminum Composite Material (ACM) Assemblies using ANSI/FM 4880," FM Global, Research Technical Report, Project ID 0003062078, December 2017 https://www.fmglobal.com/research-and-resources/research-and-testing/research-technical-reports.

16. G. Agarwal, Y. Wang, and S. Dorofeev, "Fire performance evaluation of cladding wall assemblies using the 16-ft high parallel panel test method of ANSI/FM 4880," *Fire and Materials,* vol. 45 (5), pp. 609-623, 2021. https://doi.org/10.1002/fam.2852

17. ANSI/FM 4411-2020, *American National Standard for Cavity Wall Systems*. Norwood, MA, USA: FM Approvals LLC, 2020.

18. H. Laukamp, G. Bopp, R. Grab, C. Wittwer, H. Häberlin, B. Heeckeren, S. Phillip, F. Reil, H. Schmidt, and A. Sepanski, "PV fire hazard-analysis and assessment of fire incidents," in *28th European Photovoltaic Solar Energy Conference and Exhibition, Paris*, 2013.

19. UL 4703, *Standard for Photovoltaic Wire*. Northbrook, IL: Underwriters Laboratories Inc., 2020.

20. EN 50575:2016, *Power, Control and Communication Cables. Cables for General Applications in Construction Works Subject to Reaction to Fire Requirements*. Brussels, Belgium: European Committee for Standardization, 2016.

21. Y.-C. Huang, S.-K. Lee, C.-C. Chan, and S.-J. Wang, "Full-scale evaluation of fire-resistant building integrated photovoltaic systems with different installation positions of junction boxes," *Indoor and Built Environment,* vol. 27 (9), pp. 1259-1271, 2018. https://doi.org/10.1177/1420326x17713256

22. A. Pandian, K. Bansal, D. J. Thiruvadigal, and S. Sakthivel, "Fire Hazards and Overheating Caused by Shading Faults on Photo Voltaic Solar Panel," *Fire Technology,* vol. 52 (2), pp. 349-364, 2016. https://doi.org/10.1007/s10694-015-0509-7

23. L. Fara, I. Chilibon, D. Craciunescu, A. Diaconu, and S. Fara, "Review: Heterojunction Tandem Solar Cells on Si-Based Metal Oxides," *Energies,* vol. 16 (7), p. 3033, 2023.

24. Y. Hassan, M. Orabi, A. Alshreef, O. M. Al-Rabghi, B. A. Habeebullah, A. El Aroudi, and M. A. Ismeil, "Improvement of Extracted Power of Pole Mounted Solar Panels by Effective Cooling Using Aluminum Heat Sink under Hot Weather and Variable Wind Speed Conditions," *Energies,* vol. 13 (12), p. 3159, 2020.

25. G. Masson, I. Kaizuka, E. Bosch, C. Plaza, A. Scognamiglio, A. Jäger-Waldau, J. Lindahl, and E. Blokken, "Trends in Photovoltaic Applications 2022," International Energy Agency (IEA) Photovoltaic Power Systems (PVPS) Programme, Report Number IEA PVPS T1-43:2022, 2022. https://iea-pvps.org/wp-content/uploads/2023/02/PVPS_Trend_Report_2022.pdf

26. A. Kandt, E. Hotchkiss, A. Walker, J. Buddenborg, and J. Lindberg, "Implementing Solar PV Projects on Historic Buildings and in Historic Districts," National Renewable Energy Laboratory (NREL), Technical Report Number NREL/TP-7A40-51297, September 2011. https://docs.nrel.gov/docs/fy11osti/51297.pdf

27. K. Prume and J. Viehweg, "Assessing Fire Risks in Photovoltaic Systems and Developing Safety Concepts for Risk Minimization," Office of Energy Efficiency & Renewable Energy, U.S. Department of Energy, DoE Award Number DE-EE0008073, June 2018. https://www.energy.gov/sites/default/files/2018/10/f56/PV%20Fire%20Safety%20Fire%20Guideline_Translation_V04%2020180614_FINAL.pdf

28. IEC TS 61836:2016, *Solar Photovoltaic Energy Systems - Terms, Definitions and Symbols*. Geneva, Switzerland: International Electrotechnical Commission (IEC), 2016.

29. R. Yang, Y. Zang, J. Yang, R. Wakefield, K. Nguyen, L. Shi, B. Trigunarsyah, F. Parolini, P. Bonomo, F. Frontini, D. Qi, Y. Ko, and X. Deng, "Fire safety requirements for building integrated photovoltaics (BIPV): A cross-country comparison," *Renewable and Sustainable Energy Reviews,* vol. 173 p. 113112, 2023. https://doi.org/10.1016/j.rser.2022.113112

30. M. Aram, X. Zhang, D. Qi, and Y. Ko, "A state-of-the-art review of fire safety of photovoltaic systems in buildings," *Journal of Cleaner Production,* vol. 308 p. 127239, 2021. https://doi.org/10.1016/j.jclepro.2021.127239

31. IEC 61730-1:2023, *Photovoltaic (PV) Module Safety Qualification - Part 1: Requirements for Construction*. Geneva, Switzerland: International Electrotechnical Commission (IEC), 2023.

32. IEC 61730-2:2023, *Photovoltaic (PV) Module Safety Qualification - Part 2: Requirements for Testing*. Geneva, Switzerland: International Electrotechnical Commission, 2023.

33. UL 1703, *Standard for Flat-Plate Photovoltaic Modules and Panels*. Northbrook, IL: Underwriters Laboratories Inc., 2024.

34. EN 13501-1:2018, *Fire Classification of Construction Products and Building Elements-Part1: Classification Using Data from Reaction to Fire Tests*. Brussels, Belgium: European Committee for Standardization, 2018.

35. CEN/TS 1187:2012, *Test Methods for External Fire Exposure to Roofs*. Brussels, Belgium: European Committee for Standardization, 2012.

36. ASTM E108-20a, *Standard Test Methods for Fire Tests of Roof Coverings*. West Conshohocken, PA: ASTM International, 2020.

37. UL 790, *Safety Standard Test Methods for Fire Tests of Roof Coverings*. Northbrook, IL: Underwriters Laboratories Inc., 2022.

38. D. Zeng, T. Rodrique, and D. Boardman, "Evaluation of the Effectiveness of Roof Coating for Mitigating Rooftop Photovoltaic Panel Fire," in *16th International Conference and Exhibition on Fire Science and Engineering (Interflam)*, Nr Windsor, UK, 2025.

39. S. Boddaert, P. Bonomo, G. Eder, R. Fjellgaard Mikalsen, H. Ishii, J. Kim, Y. Ko, P. Kovacs, T. Li, and X. Olano, "Fire Safety of BIPV: International Mapping of Accredited and R&D Facilities in the Context of Codes and Standards 2023," International Energy Agency (IEA), Report Number IEA-PVPS T15-15: 2023, July 2023. https://iea-pvps.org/key-topics/fire-safety-of-bipv-international-mapping-of-accredited-and-rd-facilities-in-the-context-of-codes-and-standards-2023/

40. ISO 1182, *Reaction to Fire Tests for Products -- Non-combustibility Test*. Geneva, Switzerland: International Organization for Standardization, 2020.

41. ISO 1716, *Reaction to Fire Tests for Products -- Determination of the Gross Heat of Combustion (Calorific Value)*. Geneva, Switzerland: International Organization for Standardization, 2018.

42. ISO 11925-2, *Reaction to fire tests — Ignitability of products subjected to direct impingement of flame*. Geneva, Switzerland: International Organization for Standardization, 2020.

43. EN 13823:2020, *Reaction to Fire Tests for Building Products - Building Products Excluding Floorings Exposed to the Thermal Attack by a Single Burning Item*. Brussels, Belgium: European Committee for Standardization, 2020.

44. DS 1-4, Fire Tests, *FM Property Loss Prevention Data Sheets*. Norwood, MA, 2019.

45. EN 13501-5:2016, *Fire Classification of Construction Products and Building Elements - Part 5: Classification Using Data from External Fire Exposure to Roofs Tests*. Brussels, Belgium: European Committee for Standardization, 2016.

46. N. White and M. A. Delichatsios, "Fire Hazards of Exterior Wall Assemblies Containing Combustible Components," The Fire Protection Research Foundation, Final Report, Proposal Number: FE2568, 1 June, 2014.

47. R. Stølen, T. Li, T. Wingdahl, and A. Steen-Hansen, "Large- and small-scale fire test of a building integrated photovoltaic (BIPV) façade system," *Fire Safety Journal,* vol. 144 p. 104083, 2024. https://doi.org/10.1016/j.firesaf.2023.104083

48. SP Technical Research Institute of Sweden, *SP-105 External wall assemblies and facade claddings. Reaction to fire*. 1994.

49. K. L. T. Jamison and D. A. Boardman, "A new fire performance test for cavity wall insulation," *MATEC Web of Conferences,* vol. 46 p. 02004, 2016. https://doi.org/10.1051/matecconf/20164602004

50. V. Fiandra, L. Sannino, C. Andreozzi, G. Flaminio, and M. Pellegrino, "New PV Encapsulants: Assessment of Change in Optical and Thermal Properties and Chemical Degradation after UV Aging," *Polymer Degradation and Stability,* vol. 220 p. 110643, 2024. https://doi.org/10.1016/j.polymdegradstab.2023.110643

51. K. Sadeghi, Y. Jeon, and J. Seo, "Roadmap to the Sustainable Synthesis of Polymers: From the Perspective of CO2 Upcycling," *Progress in Materials Science,* vol. 135 p. 101103, 2023. https://doi.org/10.1016/j.pmatsci.2023.101103

52. A. Dhaundiyal and D. Atsu, "Energy assessment of photovoltaic modules," *Solar Energy,* vol. 218 pp. 337-345, 2021. https://doi.org/10.1016/j.solener.2021.02.055

53. I. Subedi, T. J. Silverman, M. G. Deceglie, and N. J. Podraza, "Emissivity of solar cell cover glass calculated from infrared reflectance measurements," *Solar Energy Materials and Solar Cells,* vol. 190 pp. 98-102, 2019. https://doi.org/10.1016/j.solmat.2018.09.027

54. A. Badiee, I. A. Ashcroft, and R. D. Wildman, "The thermo-mechanical degradation of ethylene vinyl acetate used as a solar panel adhesive and encapsulant," *International Journal of Adhesion and Adhesives,* vol. 68 pp. 212-218, 2016. https://doi.org/10.1016/j.ijadhadh.2016.03.008

55. G. Oreski, A. Omazic, G. C. Eder, Y. Voronko, L. Neumaier, W. Mühleisen, C. Hirschl, G. Ujvari, R. Ebner, and M. Edler, "Properties and degradation behaviour of polyolefin encapsulants for photovoltaic modules," *Progress in Photovoltaics: Research and Applications,* vol. 28 (12), pp. 1277-1288, 2020. https://doi.org/10.1002/pip.3323

56. M. Landa - Pliquet, T. Béjat, M. Serasset, A. Descormes, E. Mofakhami, and E. Voroshazi, "Enhancing photovoltaic modules encapsulation: Optimizing lamination processes for Polyolefin Elastomers (POE) through crosslinking behavior analysis," *Solar Energy Materials and Solar Cells,* vol. 267 p. 112725, 2024. https://doi.org/10.1016/j.solmat.2024.112725

57. K. Agroui and J. Farenc, "Measurement of glass transition temperature of crosslinked EVA encapsulant by thermal analysis for photovoltaic application," *Renewable Energy,* vol. 43 pp. 218-223, 2012. https://doi.org/10.1016/j.renene.2011.11.015

58. M. Kempe, G. Jorgensen, K. Terwilliger, T. McMahon, C. Kennedy, and T. Borek, "Ethylene-Vinyl Acetate Potential Problems for Photovoltaic Packaging," in *2006 IEEE 4th World Conference on Photovoltaic Energy Conference*, Waikoloa, Hawaii, 2006, pp. 2160-2163. https://doi.org/10.1109/WCPEC.2006.279933

59. A. E.-M. A. Harb, A. Radwan, K. Elsayed, M. Sedrak, and M. Ahmed, "Influence of varying the Ethylene-Vinyl Acetate layer thicknesses on the performance of a polycrystalline silicon solar cell integrated with a microchannel heat sink," *Solar Energy,* vol. 195 pp. 592-609, 2020. https://doi.org/10.1016/j.solener.2019.11.082

60. ISO 3957, *Reaction to Fire Tests — Parallel Panel Test Method for Wall Systems — Measurement of Heat Release and Smoke Production*. Geneva, Switzerland: International Organization for Standardization, 2025.

61. J. S. Newman, "Integrated Approach to Flammability Evaluation of Polyurethane Wall/Ceiling Materials," *Journal of Cellular Plastics,* vol. 29 (5), p. 437, 1993. http://dx.doi.org/10.1177/0021955x9302900535

62. J. S. Newman and A. Tewarson, "Flame Spread Behavior of Char-Forming Wall/Ceiling Insulating Materials," *Fire Safety Science,* vol. 3 pp. 679-688, 1991. http://dx/doi.org/10.3801/IAFSS.FSS.3-679

63. J. E. J. Staggs, "Savitzky–Golay Smoothing and Numerical Differentiation of Cone Calorimeter Mass Data," *Fire Safety Journal,* vol. 40 (6), pp. 493-505, 2005. http://dx.doi.org/10.1016/j.firesaf.2005.05.002

64. M. U. A. Bromba and H. Ziegler, "Application Hints for Savitzky-Golay Digital Smoothing Filters," *Analytical Chemistry,* vol. 53 (11), pp. 1583-1586, 1981. http://dx.doi.org/10.1021/ac00234a011

65. A. Savitzky and M. J. E. Golay, "Smoothing and Differentiation of Data by Simplified Least Squares Procedures," *Analytical Chemistry,* vol. 36 (8), pp. 1627-1639, 1964. http://dx.doi.org/10.1021/ac60214a047

66. Y. Yang and C. L. Chow, "Transient temperature fields and thermal stress fields in glazing of different thicknesses exposed to heat radiation," *Construction and Building Materials,* vol. 193 pp. 589-603, 2018. https://doi.org/10.1016/j.conbuildmat.2018.10.106

67. Y. Yang, L. Miao, and C. L. Chow, "Relative significance of temperature gradient components on cracking behavior in glass panes under thermal radiation," *Applied Thermal Engineering,* vol. 131 pp. 837-848, 2018. https://doi.org/10.1016/j.applthermaleng.2017.12.060

68. FM Approvals Class Number 3210, *Examination Standard for Heat Detectors for Automatic Fire Alarm Signaling*. Norwood, MA: FM Approvals LLC, 2021.

69. S. Nam, "Intermediate-Scale Fire Test - Stepping Stone For Prediction Of Material Flamability In Real-Scale Fire Through Bench-Scale Fire Test Data," in *International Association for Fire Safety Science (AOFST)*, Cambridge, Massachusetts, USA, 2007, pp. 27-45. https://publications.iafss.org/publications/aofst/7/27/view/aofst_7-27.pdf

70. Y. Wang, X. Li, and L. Bisby, "Comparative study of thermal breakage of annealed and tempered glazing with different thicknesses under uniform radiation conditions," *Fire Safety Journal,* vol. 140 p. 103867, 2023. https://doi.org/10.1016/j.firesaf.2023.103867

71. F. Czerwinski, "Thermal Stability of Aluminum Alloys," *Materials (Basel),* vol. 13 (15), 2020. https://doi.org/10.3390/ma13153441

72. L. Miao and C. L. Chow, "A study on window plume from a room fire to the cavity of a double-skin façade," *Applied Thermal Engineering,* vol. 129 pp. 230-241, 2018. https://doi.org/10.1016/j.applthermaleng.2017.09.125

Appendix A. Additional Results — Outdoor and Indoor Tests

IR images recorded during outdoor tests of β–3mm, γ–4mm, and FlexPV modules are shown in Figs A-1 through A-3, respectively. IR images for indoor tests of γ–4mm and FlexPV modules are shown in Figs. A-4 and A-5, respectively. Operational temperatures measured during outdoor and indoor tests of α–4mm, β–3mm, γ–4mm, and FlexPV modules are listed in Tables A-1 through A-4, respectively.

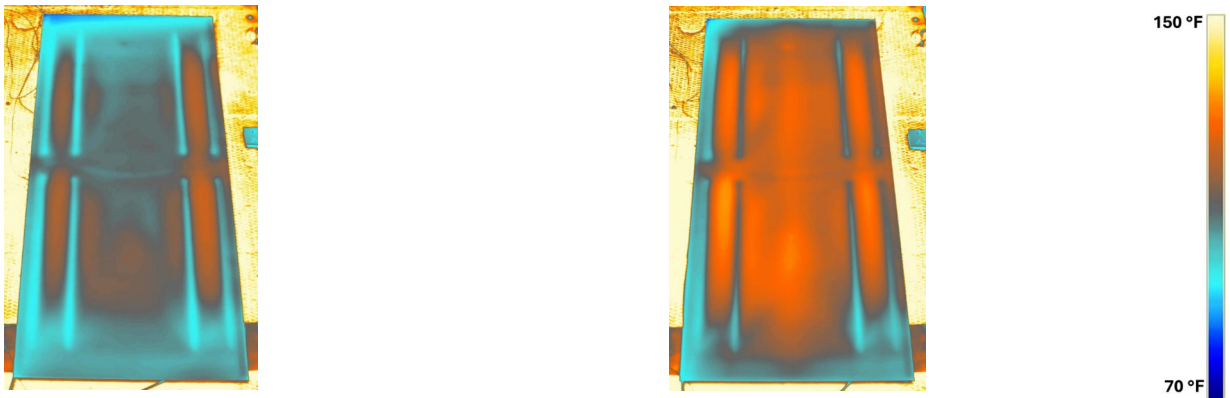

(a) OC: 126°F (52°C) (c) SC: 136°F (58°C)

Figure A-1: Temperature profiles and maximum temperature of an β–3mm module during outdoor tests at various operational stages. MP data is unavailable due to reverse current blocked by β–3mm's junction box.

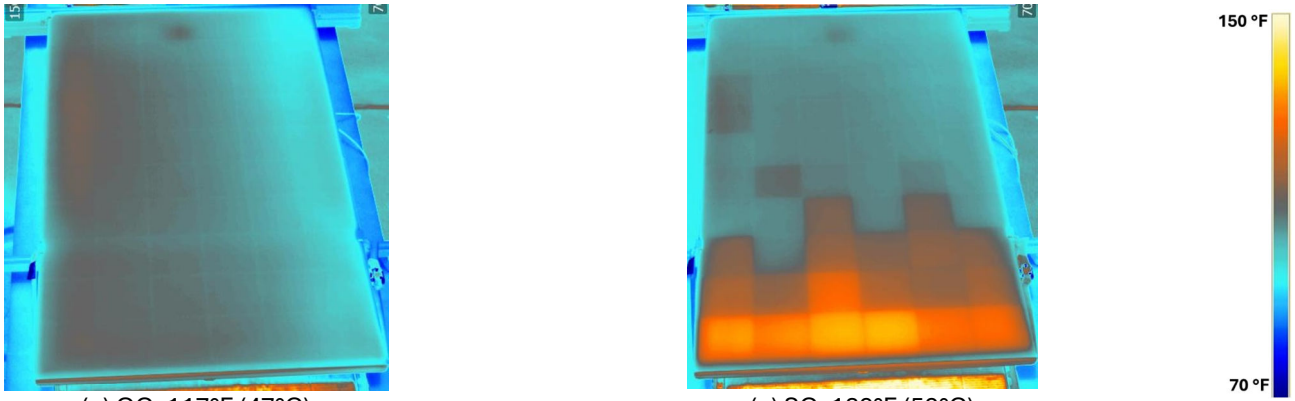

(a) OC: 117°F (47°C) (c) SC: 139°F (59°C)

Figure A-2: Temperature profiles and maximum temperature of an γ–4mm module during outdoor tests at various operational stages. The MP datafile is corrupted.

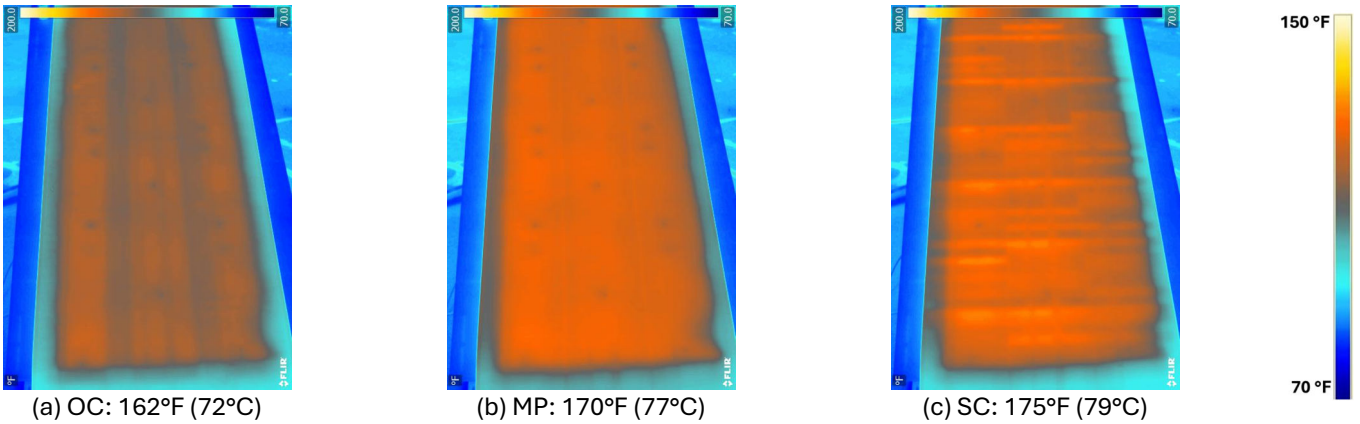

(a) OC: 162°F (72°C) (b) MP: 170°F (77°C) (c) SC: 175°F (79°C)

Figure A-3: Temperature profiles and maximum temperature of a FlexPV module during outdoor tests at various operational stages.

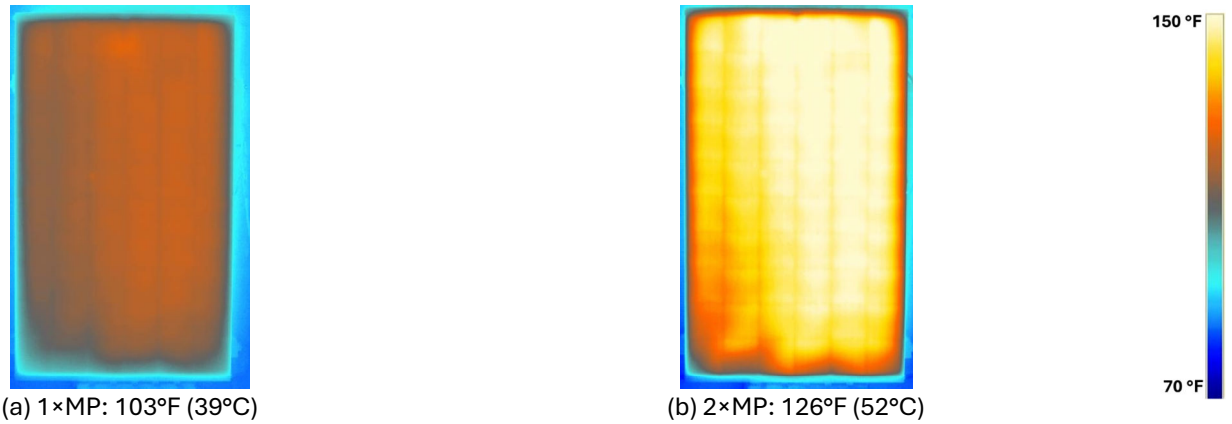

(a) 1×MP: 103°F (39°C) (b) 2×MP: 126°F (52°C)

Figure A-4: Temperature profiles and maximum temperature of γ–4mm modules during indoor tests at various power settings.

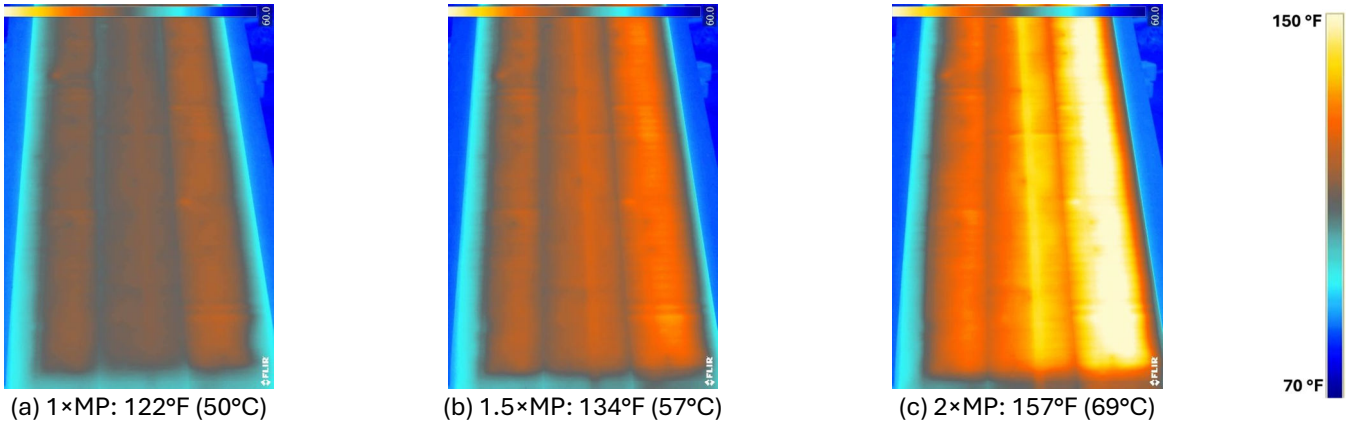

(a) 1×MP: 122°F (50°C) (b) 1.5×MP: 134°F (57°C) (c) 2×MP: 157°F (69°C)

Figure A-5: Temperature profiles and maximum temperature of FlexPV modules during indoor tests at various power settings.

Table A-1: Operational temperature measurements (°F/°C) for α–4mm module.

α–4mm	Outdoor			Indoor		
	OC	MP	SC	1×MP	1.5×MP	2×MP
Superstrate glass	120/49	144/62	196/91	104/40	119/48	136/58
Substrate glass	120/49	140/60	162/72	96/36	107/42	126/52
Insulation	115/46	128/53	139/59	91/33	100/38	112/44
Cables	111/44	128/53	130/54	89/32	100/38	111/44

Table A-2: Operational temperature measurements (°F/°C) for β–3mm module.

β–3mm	Outdoor			Indoor		
	OC	MP	SC	1×MP	1.5×MP	2×MP
Superstrate glass	126/52	NA	136/58	NA	NA	NA
Substrate glass	127/53	NA	125/52	NA	NA	NA
Insulation	129/54	NA	93/34	NA	NA	NA
Cables	128/53	NA	121/49	NA	NA	NA
NA: Not available as the β–3mm modules do not allow reverse current flow from an external power source.						

Table A-3: Operational temperature measurements (°F/°C) for γ–4mm module.

γ–4mm	Outdoor			Indoor		
	OC	MP	SC	1×MP	1.5×MP	2×MP
Superstrate glass	117/47	NA	136/58	103	NA	126
Substrate glass	115/46	130/54	126/52	NA	NA	NA
Insulation	104/40	105/41	109/43	NA	NA	NA
Cables	109/43	110/43	117/47	NA	NA	NA
NA: data not available.						

Table A-4: Operational temperature measurements (°F/°C) for FlexPV module.

FlexPV	Outdoor			Indoor		
	OC	MP	SC	1×MP	1.5×MP	2×MP
Superstrate glass	162/72	170/77	175/79	122/50	134/57	157/69
Substrate glass	NA	NA	NA	NA	NA	NA
Insulation	NA	NA	NA	NA	NA	NA
Cables	120/49	126/52	139/59	97/36	96/36	102/39
NA: Not available as the FlexPV BIPV is adhered directly to a gypsum substrate.						

Appendix B. FM 4411 Test Preparation Details

Images detailing the preparation of the 16-ft PPTs for β–3mm, γ–4mm, γ–6mm, and FlexPV systems are shown in Figs B-1 through B-4, respectively. The CWT preparation details for β–3mm and γ–4mm systems are imaged in Figs. B-5 and B-6, respectively.

(a) (b) (c) (d)

Figure B-1: 16-ft PPT setup preparation for β–3mm cavity-wall façade setup.

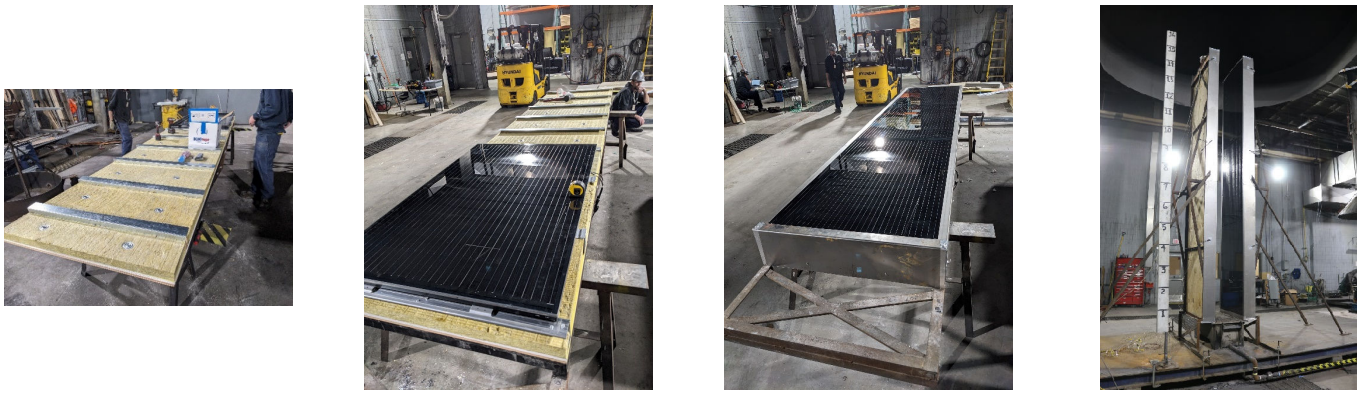

(a) (b) (c) (d)

Figure B-2: 16-ft PPT setup preparation for γ–4mm cavity-wall façade setup.

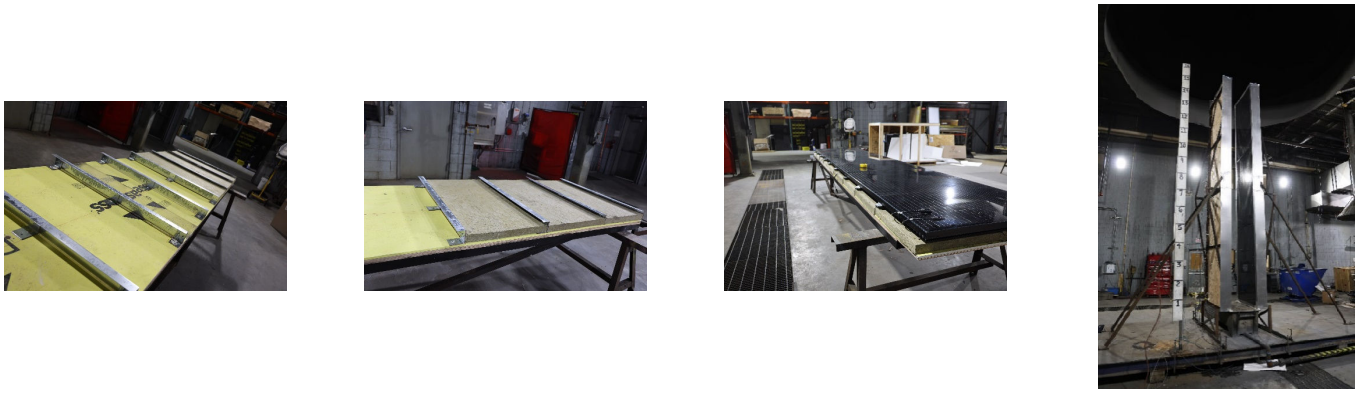

(a) (b) (c) (d)

Figure B-3: 16-ft PPT setup preparation for γ–6mm cavity-wall façade setup.

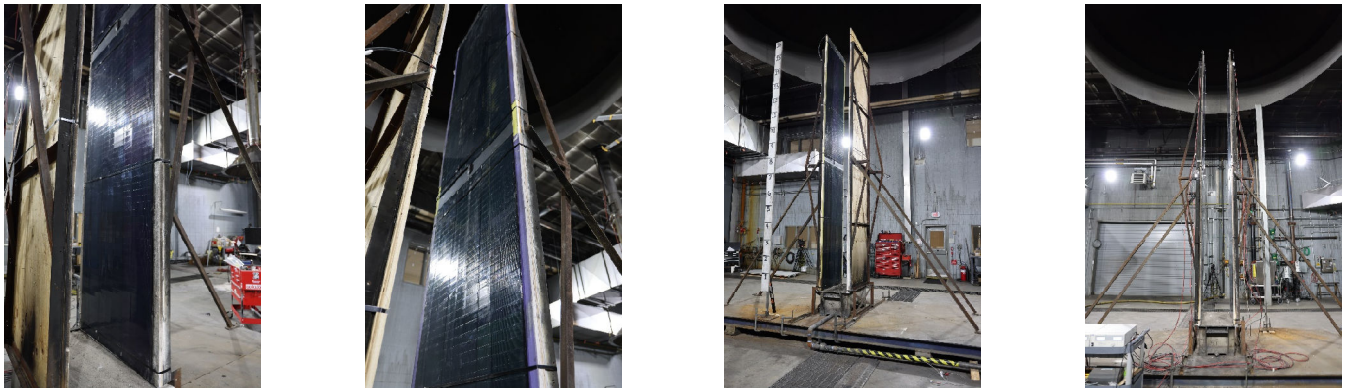

(a) (b) (c) (d)

Figure B-4: 16-ft PPT setup preparation for FlexPV cavity-wall façade setup.

(a) (b) (c) (d)

Figure B-5: 8-ft CWT setup preparation for β–3mm cavity-wall systems in OC condition.

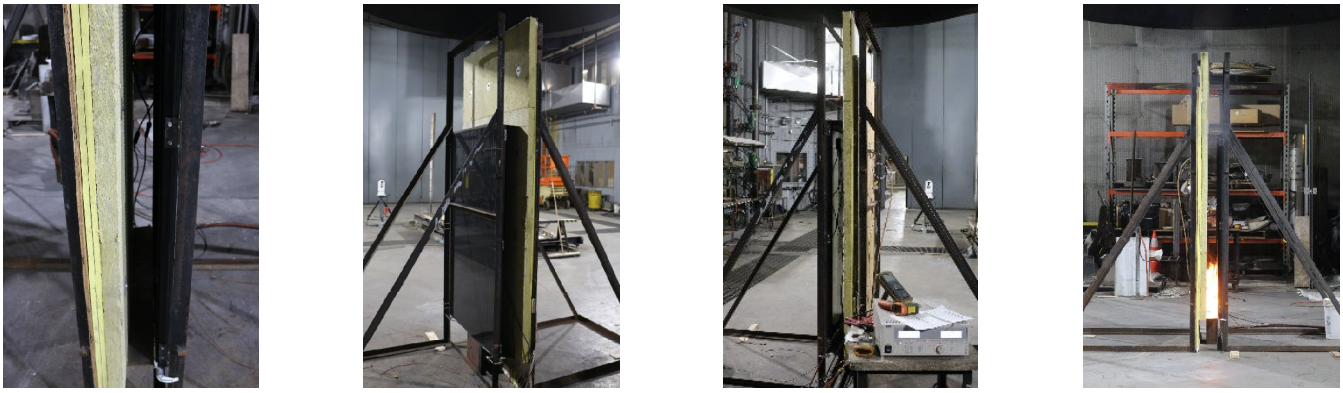

(a) (b) (c) (d)

Figure B-6: 8-ft CWT setup preparation for γ–4mm cavity-wall systems in MP condition.

Appendix C. Additional 16-ft PPT Results

Surface temperatures (STC) at 15 ft (4.6 m) height and heat flux gage (HFG) readings at 16 ft (4.9 m) height recorded during the 16-ft PPTs of α–4mm and β–3mm systems (in an open circuit, OC, condition) are shown in Figs. C-1 and C-2, respectively. Figure C-3 compares STC and HFG data for tests conducted under OC and maximum power (MP) conditions for the β–3mm system. On the other hand, Fig. C-4 compares STC and HFG data for tests conducted under OC and MP conditions for the γ–4mm system.

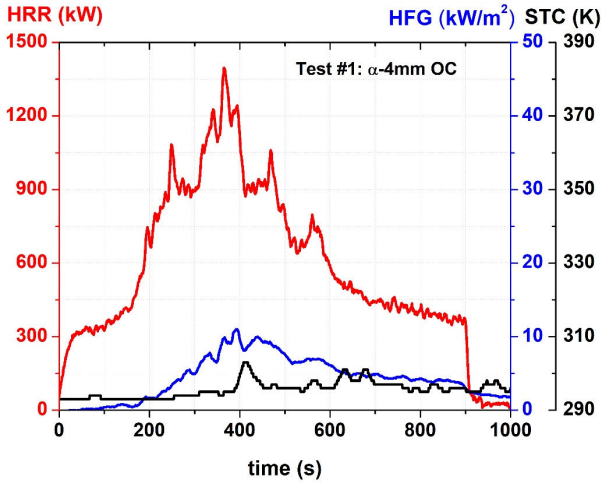

Figure C-1: Additional data for Test #1 with α–4mm OC 16-ft PPT - HRR, HFG (16 ft) and STC (15 ft) profiles.

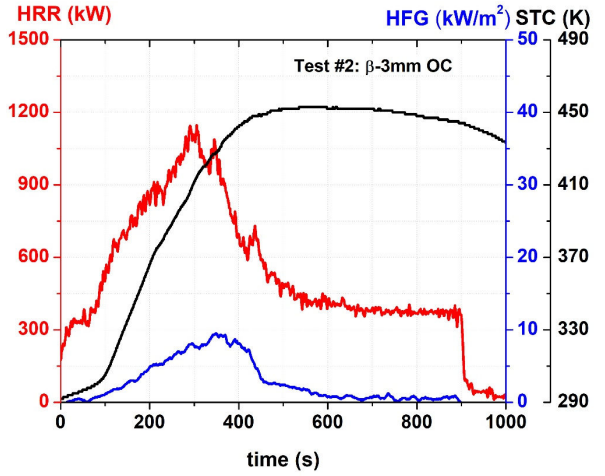

Figure C-2: Additional data for Test #2 with β–3mm OC 16-ft PPT— HRR, HFG (16 ft) and STC (15 ft) profiles.

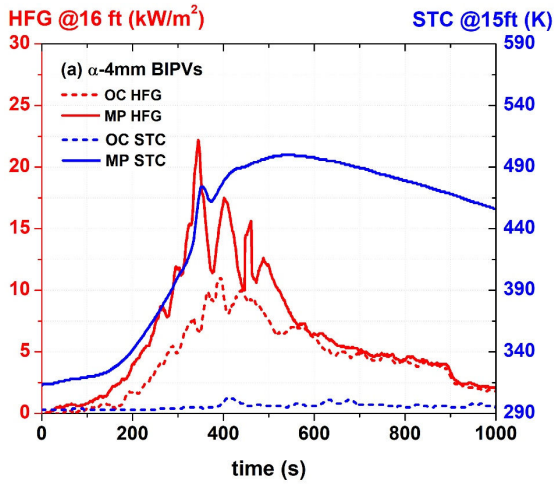

Figure C-3: Additional data for α–4mm OC and MP 16-ft PPTs — HFG (16 ft) and STC (15 ft) profiles.

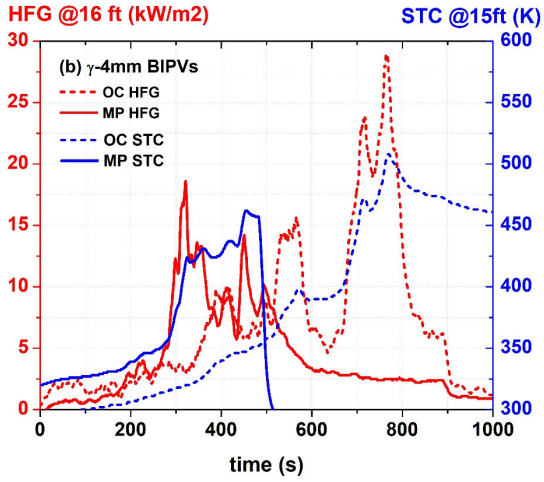

Figure C-4: Additional data for γ–4mm OC and MP 16-ft PPTs — HFG (16 ft) and STC (15 ft) profiles.

FM

@FMGlobal

InsurerFMGlobal

FM Global